A&A 675, A154 (2023)
https://doi.org/10.1051/0004-6361/202245650

Astronomy & Astrophysics

X-Shooting ULLYSES: Massive stars at low metallicity

I. Project description⋆,⋆⋆

Jorick S. Vink[1], A. Mehner[2], P. A. Crowther[3], A. Fullerton[44], M. Garcia[38], F. Martins[14], N. Morrell[16], L. M. Oskinova[26], N. St-Louis[33], A. ud-Doula[5], A. A. C. Sander[20], H. Sana[4], J.-C. Bouret[32], B. Kubátová[10], P. Marchant[4], L. P. Martins[21], A. Wofford[50], J. Th. van Loon[36], O. Grace Telford[35], Y. Götberg[37], D. M. Bowman[4], C. Erba[8], V. M. Kalari[24], M. Abdul-Masih[2], T. Alkousa[3], F. Backs[17], C. L. Barbosa[47], S. R. Berlanas[39,36], M. Bernini-Peron[20], J. M. Bestenlehner[3], R. Blomme[34], J. Bodensteiner[15], S. A. Brands[17], C. J. Evans[28], A. David-Uraz[40,43], F. A. Driessen[4,18], K. Dsilva[4], S. Geen[17,18], V. M. A. Gómez-González[26], L. Grassitelli[13], W.-R. Hamann[26], C. Hawcroft[4], A. Herrero[11], E. R. Higgins[1], D. John Hillier[9], R. Ignace[8], A. G. Istrate[49], L. Kaper[17], N. D. Kee[51], C. Kehrig[42], Z. Keszthelyi[17,19], J. Klencki[15,46], A. de Koter[17,4], R. Kuiper[23], E. Laplace[30], C. J. K. Larkin[20], R. R. Lefever[20], C. Leitherer[44], D. J. Lennon[11,12], L. Mahy[34], J. Maíz Apellániz[29], G. Maravelias[48,52], W. Marcolino[41], A. F. McLeod[6,7], S. E. de Mink[46,17], F. Najarro[38], M. S. Oey[25], T. N. Parsons[22], D. Pauli[26], M. G. Pedersen[27], R. K. Prinja[22], V. Ramachandran[20], M. C. Ramírez-Tannus[45], G. N. Sabhahit[1], A. Schootemeijer[13], S. Reyero Serantes[26], T. Shenar[17], G. S. Stringfellow[31], N. Sudnik[33], F. Tramper[4], and L. Wang[53]

(Affiliations can be found after the references)

Received 8 December 2022 / Accepted 5 May 2023

ABSTRACT

Observations of individual massive stars, super-luminous supernovae, gamma-ray bursts, and gravitational wave events involving spectacular black hole mergers indicate that the low-metallicity Universe is fundamentally different from our own Galaxy. Many transient phenomena will remain enigmatic until we achieve a firm understanding of the physics and evolution of massive stars at low metallicity (Z). The *Hubble* Space Telescope has devoted 500 orbits to observing ~250 massive stars at low Z in the ultraviolet (UV) with the COS and STIS spectrographs under the ULLYSES programme. The complementary X-Shooting ULLYSES (XShootU) project provides an enhanced legacy value with high-quality optical and near-infrared spectra obtained with the wide-wavelength coverage X-shooter spectrograph at ESO's Very Large Telescope. We present an overview of the XShootU project, showing that combining ULLYSES UV and XShootU optical spectra is critical for the uniform determination of stellar parameters such as effective temperature, surface gravity, luminosity, and abundances, as well as wind properties such as mass-loss rates as a function of Z. As uncertainties in stellar and wind parameters percolate into many adjacent areas of astrophysics, the data and modelling of the XShootU project is expected to be a game changer for our physical understanding of massive stars at low Z. To be able to confidently interpret *James Webb* Space Telescope spectra of the first stellar generations, the individual spectra of low-Z stars need to be understood, which is exactly where XShootU can deliver.

Key words. stars: atmospheres – stars: early-type – stars: winds, outflows – stars: evolution – methods: observational – galaxies: dwarf

1. Introduction

We find ourselves amidst a scientific revolution: gravitational wave (GW) observatories will soon be detecting black hole (BH) mergers as frequently as once per day. To interpret these events, we need to comprehend massive stars in low-metallicity environments (Abbott et al. 2020). This is also crucial for other fields of astrophysics, including feedback processes (e.g. Doran et al. 2013), star formation, interstellar medium (ISM) physics, supernovae (SNe), and cosmology. To enable progress in these research areas, we need to uniformly sample the relevant parameter space for massive OB stars, including spectral type, luminosity class, and metallicity (Z).

The *Hubble* Space Telescope (HST) has dedicated 1000 orbits to the Director's Discretionary Time project Ultraviolet Legacy Library of Young Stars as Essential Standards (ULLYSES; Roman-Duval et al. 2020)[1], making this the largest HST programme ever conducted. ULLYSES is compiling an ultraviolet (UV) spectroscopic Legacy Atlas of about 250 OB stars in low-Z regions[2]. Due to their proximity, the Large and Small Magellanic Clouds (LMC and SMC) are the best low-Z laboratories for massive star studies, with respectively 50% and 20% $Z_\odot$. They are ideal for studying spatially resolved populations of low-Z massive stars to make a leap towards understanding the early Universe. As a pilot study, several stars at sub-SMC metallicities (in Sextans A and NGC 3109; ~10% $Z_\odot$) are also included. The aim is to uniformly cover all spectral sub-types from O2 to B9 and to observe all luminosity classes with spectral types

⋆ Table B.1 and full Table B.2 are available at the CDS via anonymous ftp to cdsarc.cds.unistra.fr (130.79.128.5) or via https://cdsarc.cds.unistra.fr/viz-bin/cat/J/A+A/675/A154

⋆⋆ Based on observations collected at the European Southern Observatory under ESO programme 106.211Z.001.

[1] https://ullyses.stsci.edu

[2] The ULLYSES programme is also compiling high-quality far-UV, near-UV, and optical spectra of young, low-mass T Tauri stars in our Galaxy.

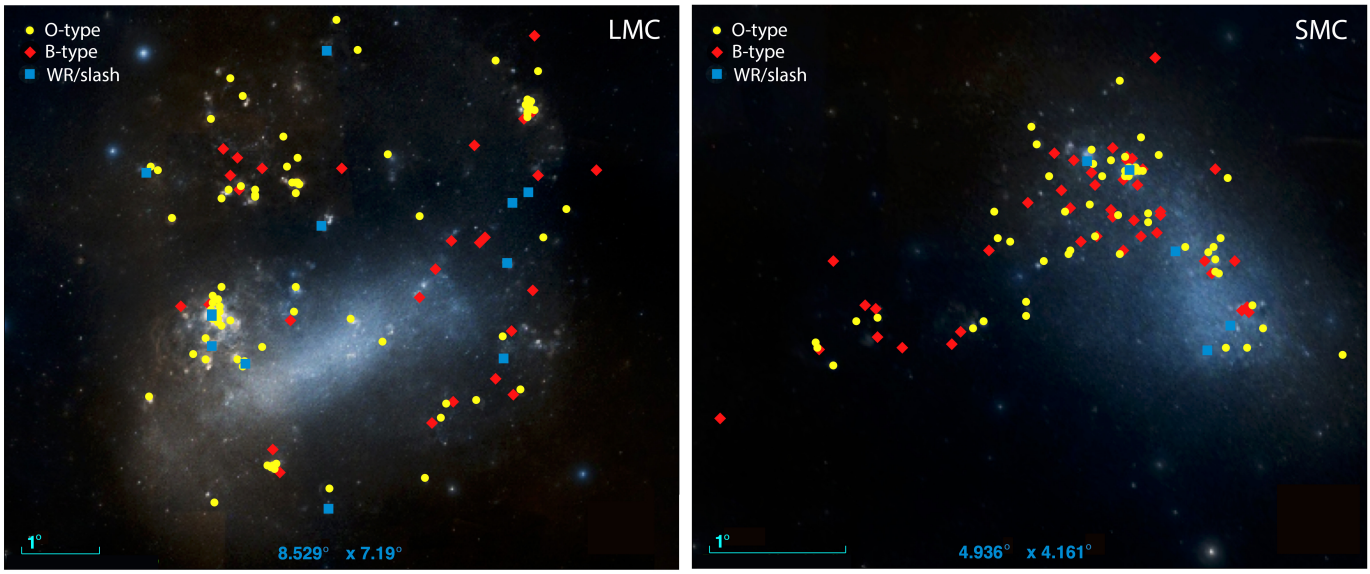

Fig. 1. Positions of the ULLYSES/XShootU sources in the LMC (left) and SMC (right). Yellow dots are O-type stars, red diamonds are B-type stars, and blue squares are WR and WR-like Of/WR 'slash' stars. We note that the two images have different spatial scales. This figure was made with the Aladin Sky Atlas (Bonnarel et al. 2000); the background consists of DSS2 colour images.

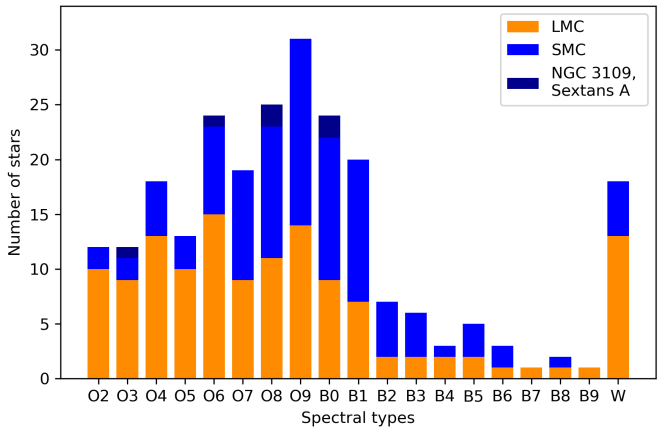

Fig. 2. Distribution of the spectral types in ULLYSES. For the ten known binaries in the sample, only the primary component is accounted for. The category labelled 'W' includes WR and WR-like 'slash' stars.

O2−B1.5 for both LMC and SMC metallicities, a total of ~250 stars (Figs. 1 and 2).

Although massive stars emit the bulk of their light at UV wavelengths, the optical region remains the cornerstone of spectroscopic analysis studies. The UV regime is very useful for determining the iron (Fe) abundance and obtaining information on wind parameters, such as the terminal velocity (v_∞). The optical regime is crucial for determining the basic stellar parameters, such as effective temperature ($T_{\rm eff}$), surface gravity ($\log g$), and abundances (Hillier 2020; Simón-Díaz 2020; Brands et al. 2022) Key information on wind clumping and mass-loss rates ($\dot{M}$) only become reliable when optical and near-infrared (NIR) observations are added. Knowledge of the NIR regime is also critical for observations with instrumentation on the *James Webb* Space Telescope (JWST) and the extremely large telescopes, which will predominately shift our focus to longer wavelengths. Despite the great potential of ULLYSES to transform our knowledge of massive stars, this Legacy dataset is not complete without observations in the optical and NIR regimes. Thus, the X-Shooting ULLYSES (XShootU)[3] project was conceived to obtain complementary high-quality spectra of the ULYSSES targets with X-shooter at the European Southern Observatory (ESO) Very Large Telescope (VLT; Vernet et al. 2011).

The optical Large VLT-FLAMES Survey of massive stars (PI: S.J. Smartt) and its successor, the VLT-FLAMES Tarantula Survey (VFTS; PI: C.J. Evans), tackled many science questions, including the Z dependence of stellar wind mass-loss rates (Mokiem et al. 2007b) and the rotation velocities of massive stars (Ramírez-Agudelo et al. 2013). The surface nitrogen (N) abundance of most massive stars in the Magellanic Clouds seemed to be consistent with theoretical predictions, but a significant fraction of stars (20%−40% depending on sample and metallicity) showed chemical enrichment that is either too strong or too weak (e.g. Hunter et al. 2008a; Przybilla et al. 2010; Maeder et al. 2014; Grin et al. 2017).

The absolute mass-loss rates of massive OB and Wolf-Rayet (WR) stars are still uncertain (e.g. Sundqvist et al. 2019; Sander et al. 2020; Ramachandran et al. 2019; Marcolino et al. 2022; Rickard et al. 2022). According to evolutionary models, the bulk of the mass loss could occur during the B supergiant phase rather than during the preceding O-star phase (Groh et al. 2014). The Z dependence of mass-loss behaviour in this cooler regime is highly complex, involving various mass-loss discontinuities as a function of temperature (bi-stability jumps; Petrov et al. 2016), and is critical in predicting BH masses as a function of Z (Belczynski et al. 2010) as well as GW mergers (Kruckow et al. 2016).

The combined UV and optical XShootU project was motivated to address these science questions as well as a large variety of additional questions concerning massive stars at low Z. The project will derive accurate stellar and wind parameters, such as effective temperatures, luminosities, gravities, abundances, and mass-loss rates. This will establish whether mass-loss rates decrease with lower Z, as predicted (Vink et al. 2001; Kudritzki 2002) and empirically supported for relatively small LMC and SMC VLT-FLAMES survey samples

[3] https://massivestars.org/xshootu/

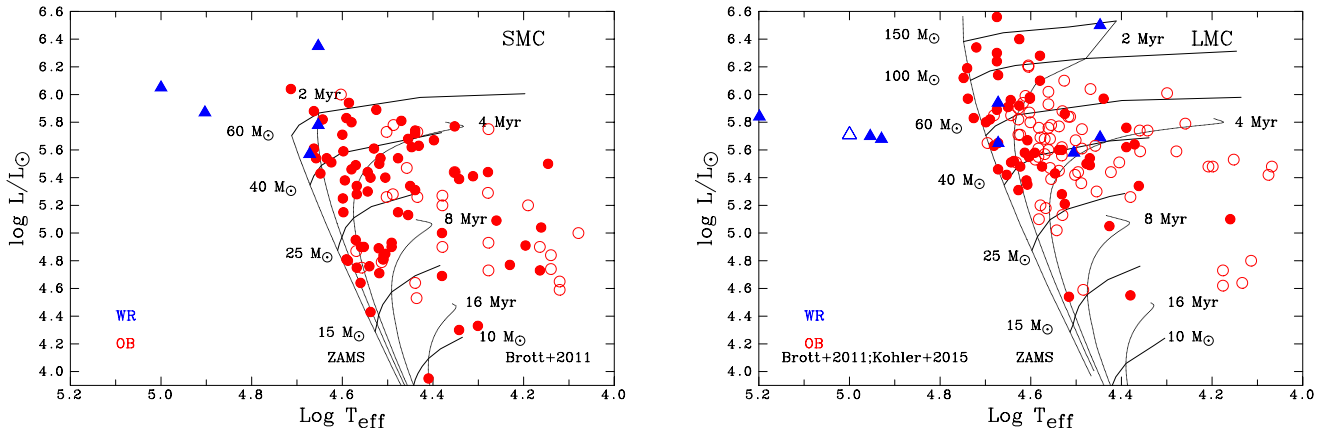

Fig. 3. HR diagrams of the ULLYSES SMC and LMC targets. Stellar parameters are based on contemporary literature from Table B.2 (filled symbols) or spectral type calibrations (open symbols). For known binary and multiple systems, only primaries are indicated. Calibrations used are Doran et al. (2013) for O-type stars in both galaxies, Dufton et al. (2019), Trundle et al. (2004), and Trundle & Lennon (2005) for SMC B-type stars, and Dufton et al. (2018), Garland et al. (2017), McEvoy et al. (2015), and Urbaneja et al. (2017) for LMC B-type stars. Evolutionary tracks (solid lines) and isochrones (dotted lines) for non-rotating massive stars at 0.5 $Z_\odot$ and 0.2 $Z_\odot$ are from Brott et al. (2011), supplemented by tracks for very massive stars in the LMC from Köhler et al. (2015).

(Mokiem et al. 2007b; Ramachandran et al. 2019). Moreover, feedback parameters involving wind momenta, wind kinetic energy, and ionising fluxes are key ingredients for building the next generation of spectral population synthesis models that may be applied to extra-galactic surveys, such as CLUES (Sirressi et al. 2022), the COS Legacy Spectroscopic SurveY (CLASSY; Berg et al. 2022), the HST spectroscopic survey of star-forming galaxies in the local Universe, and future projects. Bright early-type stars are also excellent probes of ISM conditions (van Loon et al. 2013). We expect many spin-off projects that use XShootU and ULLYSES data, including the derivation of the extinction law for which X-shooter's wide spectral range is particularly useful.

In this work we present the XShootU project. The science requirements are described, as are initial results on data reduction and data analysis processes. We show how the legacy spectroscopic dataset of ULLYSES and XShootU can increase our knowledge of massive stars at low Z. The organisation of the XShootU collaboration is described in the appendix. Already published data (Table B.2, plotted in Fig. 3) may naively suggest that properties of LMC and SMC stars are known, but these pre-ULLYSES results have been derived for relatively small and heterogeneous datasets, and gaps are evident. To make matters worse, spectral analyses that derive stellar properties have also been heterogeneous, as different authors have not only used different tools, distances, and baseline abundances, but also different wavelength ranges.

To make progress, not only do the spectroscopic datasets need to be uniform – as provided by ULLYSES and XShootU – but so does the spectral analysis approach. To give an example, determining the $\dot{M} - Z$ relationship not only requires accurate mass-loss rate determinations, but also reliable stellar parameters, such as luminosities, to compare the $\dot{M}$ from one star with one set of stellar properties in one particular galaxy to the mass-loss rate from another star in another galaxy. A uniform data and analysis approach is at the heart of the XShootU project.

2. XShootU science requirements

In order to build better population synthesis models of massive stars in low-Z environments, such as those at high redshift studied with JWST, we require (i) more complete spectral libraries and (ii) more reliable stellar evolution models for low-Z stars. The former involves the construction of more accurate model atmospheres, but the latter implies a better handle on the behaviour of wind mass loss over a multi-dimensional parameter space, including Z. The key line driver of the inner winds that sets $\dot{M}$ of massive OB stars is iron (Fe), while intermediate mass elements such as C, N, and O dominate the outer winds, setting the terminal velocity (Vink et al. 1999; Puls et al. 2000). While high redshift galaxies may have different [α/Fe] ratios compared to local low-Z galaxies, non-solar [α/Fe] ratios should have very little impact on the expected mass-loss rate, as long as one correctly interprets low Z as having low Fe contents (see for instance Table 5 in Vink et al. (2001) for conversions between O and Fe).

One potential concern is whether the local low-Z LMC and SMC at 0.5 $Z_\odot$ and 0.2 $Z_\odot$ are sufficiently metal-poor to gain insight into low-Z stellar evolution in high-redshift galaxies. In order to make the case that the SMC indeed has a sufficiently low Fe-contents to provide key insights into the early Universe, we showcase a number of MESA stellar evolution models (see Appendix A.5) in Fig. 4. The plot indicates that a rapidly rotating massive star at LMC metallicity still shows classical redwards evolution, just like in the Milky Way, but that already the one-fifth solar SMC metallicity is sufficiently low to undergo bluewards chemically homogeneous evolution (CHE), similar to even lower-Z stars at one-tenth solar. The Galactic model loses as much as a third of its initial 50 $M_\odot$ mass already on the main-sequence, while the SMC and lower-Z models lose of the order of 10% or less. Moreover, while the Galactic and LMC models completely spin down during the main sequence (the Galactic model drops below the minimum observable $v \sin i$ value of 100 km s^{-1} after 3 Myrs, while the LMC star can delay this to 4.5 Myrs), the SMC and lower-Z models hardly spin down at all. In fact, the SMC and lower-Z model evolve towards critical rotation, rather than away from it. In other words, the SMC is an ideal test-bed for gaining an understanding of the physical difference between the high-Z and the low-Z Universe.

The results displayed in Fig. 4 may naively give the impression that stellar evolution is already well understood, but this is not the case, and the stellar evolution and population synthesis models are only as good as the input physics. In this parameter space those are predominately given by the assumed amounts of interior mixing and wind mass loss. It is commonly

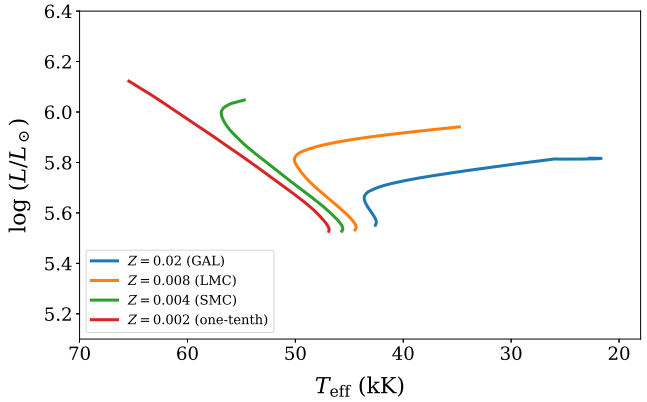

Fig. 4. Main-sequence MESA stellar evolution models of a rapidly rotating ($v \sin i$ = 550 km s^{-1}) 50 $M_\odot$ star for a range of metallicities. The Galactic and LMC models show traditional redward evolution, while the SMC and even lower-Z (one-tenth solar) models start to show blueward chemical homogeneous evolution. The models employ Vink et al. (2000, 2001) mass-loss rates and assume a moderate amount of core overshooting, with a value of α_{ov} of 0.335, similar to the Brott et al. (2011) models.

assumed that the only parameters setting the mass-loss rate are the stellar luminosity and the metallicity, but in the oft-used mass-loss recipe of Vink et al. (2000, 2001) parameters such as stellar mass, and effective temperature – including the B supergiant regime below the bi-stability jump – also play a crucial role. Therefore, in order to make progress on the accuracy of stellar evolution models at low Z we firstly require large samples of wind parameters offered by the ULLYSES sample. Secondly, in order to test these in different parts of the Hertzsprung-Russell (HR) diagram, the underlying stellar parameters also need to be robust. Thirdly, in order to test the role of rotational mixing for a range of metallicities we require stellar abundances.

Starting with the third requirement, massive stars undergo H-burning via the CNO cycle, and in the first instance the core nitrogen (N) abundance is expected to increase by an order of magnitude at the expense of carbon (C; Brott et al. 2011; Ekström et al. 2012). Mixing can bring enhanced N to the surface, which is especially relevant for testing the physics of rotational mixing in stellar evolution models. Factors of 2–10 in N enhancement and C depletion are realistically measurable from UV and optical spectroscopy as discussed in Sect. 4. For the stellar parameters, effective temperatures need to be accurate to within 5–10%, which is routinely achieved in non-local thermodynamic equilibrium model (NLTE) atmosphere modelling. More cumbersome is the estimated $\log g$ that determines the spectroscopic mass. In Sect. 4 we show that in order to be able to derive accurate $\log g$ the UV alone does not suffice, and optical Balmer lines are mandatory (see below). Arguably the least well-constrained parameter is the wind mass-loss rate. While UV P Cygni lines offer relatively accurate values of the terminal wind velocity, ~10% (Prinja et al. 1990), uncertainties in empirical mass-loss rates are about an order of magnitude due to the roles of, respectively, micro-clumping and macro-clumping (Fullerton et al. 2006; Oskinova et al. 2007; Sundqvist et al. 2018) Clearly, such huge uncertainties are not acceptable when building reliable stellar evolution and populations synthesis models. From our experience in stellar modelling, such as the experiments performed in Fig. 4, we conclude that we need the mass-loss rate to be accurate to 0.3 dex.

As the mass-loss rate is a multi-variate function of stellar parameters, such as L, M, and $T_{\rm eff}$, the accuracy requirements on the stellar parameters need to be at least as good as those for the mass-loss rate. Accuracies on $T_{\rm eff}$ are easily within 10%, though precisions of 1 kK are sometimes quoted. Similarly, $\log L$ precisions of 0.1 dex are feasible. However, the real culprit is the stellar mass, M, which can be obtained from $\log g$ spectroscopically but which has a long history of uncertainty, culminating in systematic differences between these spectroscopic masses and evolutionary masses of the order of a factor of ~2 (Herrero et al. 1992). In Sect. 4 we show that the optical regime is absolutely critical to measure $\log g$.

3. XShootU data description

3.1. Target selection

The first objective of the XShootU project is to create a homogeneous legacy atlas of similar quality and scope as that of ULLYSES. The target sample contains 132 LMC stars, 106 SMC targets, and 6 very-low-Z stars in Sextans A and NGC 3109 (Roman-Duval et al. 2020; see Table B.1 of this paper).

Most ULLYSES targets are O-type stars (154), but B-type stars (72), and WR/slash stars (18) are also included. Figure 1 displays the positions of the targets on the sky, and Fig. 2 shows the distribution of spectral types. The SMC targets have masses in the range of 10−60 $M_\odot$, whereas the LMC targets have masses in the range of 15−150 $M_\odot$. A subset of the ULLYSES targets have previously been spectroscopically analysed (see Table B.2). These heterogeneous pre-ULLYSES data are presented in the HR diagram in Fig. 3 (filled symbols). Estimated parameters for targets lacking contemporary analyses are also shown (open symbols).

XShootU obtained a complementary dataset over the optical to NIR wavelength range for all ULLYSES targets that have not previously been observed with X-shooter. This resulted in a sample of 129[4] LMC stars and 103 SMC stars. In addition, three very low-Z stars were included in the sample.

The ULLYSES and XShootU datasets are not taken simultaneously in time, although, apart from a few exceptions, the vast majority of ULLYSES sources are not known variables. In reality, most stars are variable to some level, so care still needs to be taken when interpreting the data, but we do not anticipate this to be a massive issue. Existing ESO Science Archive Facility data are part of both spectroscopic and time-dependent aspects of XShootU. Over half of the ULLYSES targets have no previous high-quality optical spectra. Several have been observed with UVES (15%) and/or FLAMES (~50%), but the wavelength coverage of these FLAMES data is limited. Using (limited) time-sequence data, we searched for binary signatures, and in some cases be capable of disentangling spectra of multi-component systems (Mahy et al. 2020).

3.2. XShootU observing strategy

3.2.1. Wavelength coverage

ULLYSES obtained moderate resolution spectra of OB stars with selected wavelength settings of the COS G130M, COS G160M, STIS E140M, COS G185M, and STIS E230M gratings in the far- and near-UV during HST cycles 27−29. In order to complement this UV range, similar quality optical/NIR

[4] These numbers are slightly different as a few archival X-shooter datasets were available.

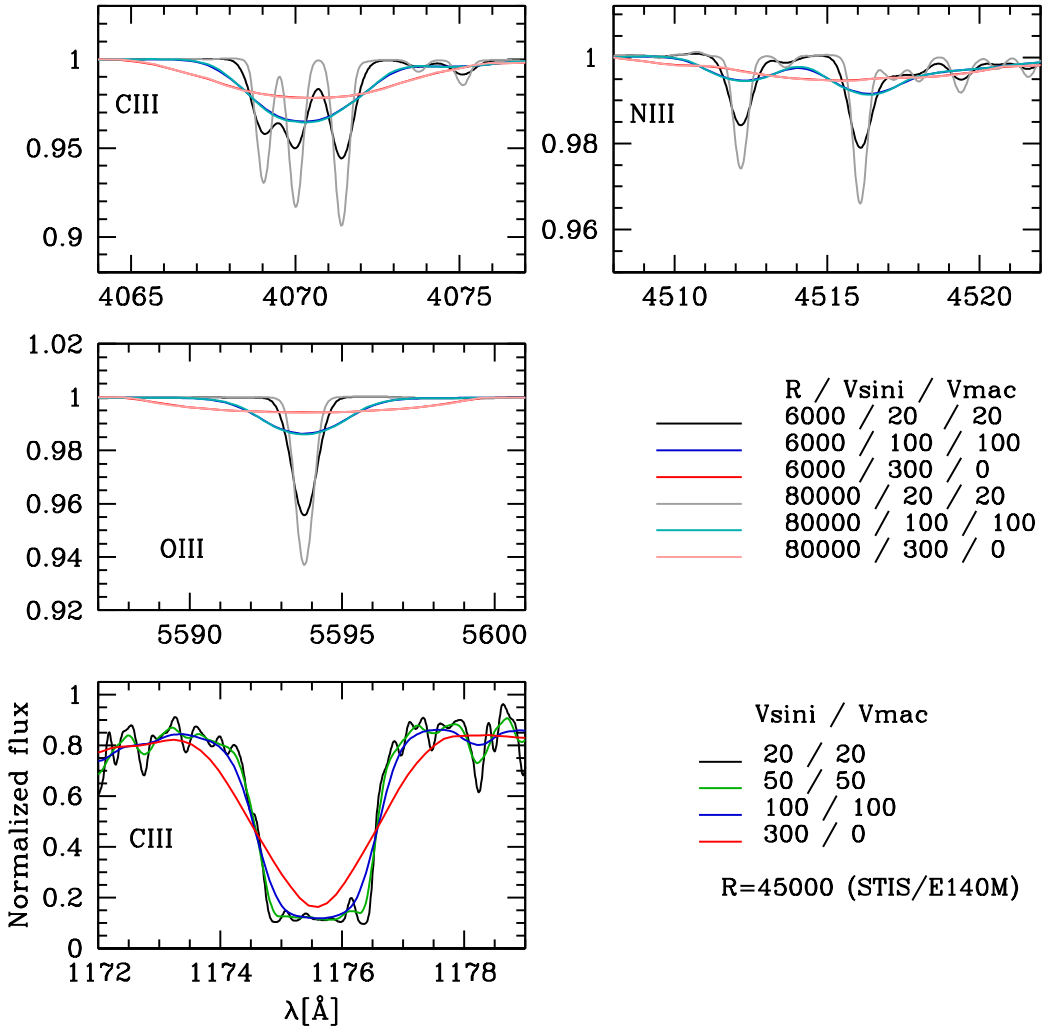

Fig. 5. Effect of spectral resolution and rotational velocity on three sets of optical lines classically used to determine C, N, and O abundances. In each panel, the initial CMFGEN model has $T_{\rm eff}$ = 31 000 K, $\log g$ = 3.6 and 0.2 $Z_\odot$. The model is degraded to a resolution of either 6000 (typical for our X-shooter UVB spectra) or 80 000 and further convolved with three rotational velocities (20, 100, and 300 km s^{-1}). No additional macro-turbulent broadening is considered. Also plotted is the UV C III 1176 line. Here the spectral resolution is that of the STIS E140M grating ($R \sim 45\,000$).

spectroscopy was carried out with the X-shooter instrument. This slit-fed (11″ slit length) spectrograph provides simultaneous coverage of the wavelength region between 300−2500 nm, divided into three arms; UVB ($300 \lesssim \lambda \lesssim 500$ nm), VIS ($500 \lesssim \lambda \lesssim 1000$ nm), and NIR ($1000 \lesssim \lambda \lesssim 2500$ nm). X-shooter's wide wavelength coverage made it the instrument of choice for the purpose of building an optical-NIR legacy dataset.

3.2.2. Spectral resolution

The X-shooter slit widths were chosen to obtain a spectral resolution of R = 5000−10 000, required for estimating the stellar parameters. Each target was observed with a set of 0.″8 (UVB, R = 6700), 0.″7 (VIS, R = 11 400), and 0.″6 (NIR, R = 8100) slit widths, matching also the average seeing conditions on Paranal. The slit position angle was set by default to the parallactic angle, but when necessary a fixed position angle on the sky was used to optimally prevent nearby sources from entering the slits.

Figure 5 illustrates that although the spectral resolution is only medium, the determination of surface abundances, including nitrogen (N), carbon (C), and oxygen (O), should be feasible. It is the projected rotational velocity of some of the stars that will limit such studies. The higher $v \sin i$, the broader the lines, which become challenging to identify at very high $v \sin i$. Even with a S/N around 100 (see the justification below) most lines would be undetectable at high $v \sin i$. On the other side of the distribution, lines are only partially resolved at low $v \sin i$. Consequently, the determination of accurate low $v \sin i$ values is not feasible, and additional higher spectral resolution data are needed for this subset (see Appendix A.11 for a description of auxiliary *Magellan*/MIKE data), although the combined analysis of optical and UV lines can partially alleviate this limitation. The bottom panel of Fig. 5 illustrates the effect of rotational broadening of C III 1176, a line complex relevant for the determination of $v \sin i$ (e.g. Bouret et al. 2013). Above 100 km s^{-1}, the components of the multiplet are blended, while at lower rotational velocities they are resolved individually.

3.2.3. Signal-to noise ratio

Some VLT instruments provide higher spectral resolution in certain wavelength regimes (e.g. UVES), but to build a

homogeneous database with a wide spectral coverage could only be achieved with X-shooter. In addition to the wide wavelength coverage, a high signal-to-noise ratio (S/N) in addition to sufficient spectral resolution are essential to determine the fundamental stellar parameters and the abundances for various temperature regimes populated by OB and WR stars. For the preparation of the X-shooter proposal, we estimated the required S/N, experimenting on a typical SMC mid-O dwarf/giant with CMFGEN model spectra degraded to X-shooter's spectral resolution. We found that the determination of basic stellar parameters such as $T_{\rm eff}$ and $\log g$ became prohibitive for quantitative interpretation if the S/N drops below 100 per resolution element. To ensure the maximal scientific return of XShootU, we achieved a S/N of >100 in the continuum in the UVB and VIS for all Magellanic Cloud targets.

3.3. Data reduction

A detailed description of the data reduction is provided in a paper associated with Data Release 1 (DR1; Sana et al., in prep., hereafter XShootU II). Here, we provide a brief summary, focusing on the UVB and VIS spectra. The data reduction of the NIR spectra requires additional efforts and will become part of DR2.

The initial data reduction was performed using the ESO X-shooter pipeline v3.5.0 (Goldoni 2011). The pipeline carried out the standard steps of bias, flat, wavelength calibration, spectral rectification, cosmic ray removal, sky subtraction, flux calibration, and extraction of a 1D spectrum. The wavelength calibration was performed using a physical model, that is to say, the transformation from pixel to lambda space was optimised through the analysis of a multi-pinhole ThAr (UVB, VIS) or penray (NIR) lamp frame. The predicted positions of the lines were fitted using a 2D Gaussian to recover the actual positions on the frame.

The pipeline-reduced data were subsequently flux calibrated using a set of six standard stars observed during the same or adjacent nights. We found that the stellar models used by the public pipeline (Moehler et al. 2014) resulted in small (of the order of a few percent) changes in the Balmer line profiles depending on the standard star. This potentially impedes accurate $\log g$ measurements. In addition, the spectral energy distribution for some of the standard stars could be optimised. We decided to use new stellar models and new fit points to derive the response, starting with models used by HST for their fundamental flux standards GD 71 and GD 153 (Bohlin et al. 2020)[5]. We then reduced observations of the other five standard stars taken between October 2020 and April 2021 as if they were science objects, with the response determined by close-in-time observations of GD 71. Those spectra were then co-added to create high S/N spectra that were used to derive improved stellar models. The XShootU spectra were obtained with narrow slits. To obtain absolute flux calibrated spectra, corrections were applied for slit losses due to seeing and image quality across the detector and by re-scaling to existing photometry. The achieved accuracy is typically better than 5%.

Telluric correction was performed using the molecfit tool v3.0.3 (Smette et al. 2015; Kausch et al. 2015) for the VIS arm and generally leads to good results. For the Magellanic Cloud targets, we fitted the atmospheric model directly to the science spectra, as the S/N on the continuum is high enough to ensure a better correction than using a telluric standard star to compute the model. The regions with very deep O_2 telluric absorption lines at ~760 nm and sometimes the one at ~690 nm are poorly corrected and the correction of the H_2O bands at ~950 nm leaves strong residuals. The correction from telluric lines around the [OI] 6300 Å line is always good.

Results of the data reduction are shown in Fig. 6. Here a sample of reduced X-shooter spectra is presented to highlight a sequence from the earliest to the latest spectral types for supergiant and dwarf targets. The spectra shown are single-epoch in order to avoid confusion in co-added spectra due to potential variability. Telluric correction (grey regions) and proper cosmic-ray removal was not performed for this plot, but will become part of DR1 (XShootU II). An example of an O4 supergiant spectrum is shown in Fig. 7 on a improved scale, focused on wavelength regions in which telluric corrections are not needed.

4. Multi-wavelength analyses

In Sect. 2 we show that the low-Z environment of the SMC can be considered rather characteristic of the early Universe, with low mass-loss rates, and the potential for rapid rotation and blueward evolution, while the LMC sample is more characteristic of today's Universe, with higher mass-loss rates, slower rotation, and classical redward stellar evolution. In reality, the situation is more complex, as the mass-loss rates is a function of $\dot{M} = f(Z, L, M, T_{\rm eff}, v \sin i)$, which implies we need to obtain stellar and wind parameters over a large parameter space, including not only the O-star regime, but also the B supergiant regime, where the bi-stability jump may increase mass-loss rates (Vink et al. 1999), or not (Björklund et al. 2021). Moreover, stellar evolution models depend on interior mixing, and stellar abundances can be utilised to test the efficiency of (rotational) mixing.

4.1. Diagnostics in the UV and optical range

In the optical range, He/H abundances can only be determined from the optical since H/He lines in the UV are dominated by strong interstellar features (e.g. Lyman alpha) so the Pickering-Balmer lines in the optical are critical for the He/H ratio.

Abundances of C, N, and O can in principle be determined from the UV range only (e.g. Bouret et al. 2003, 2013) but most lines are also sensitive to winds, especially as one moves away from the main sequence. Figure 8 shows an example where winds are sufficiently weak for such a determination. The plot also highlights that the optical range contains more lines from these elements, and these lines depend far less on wind properties than those in the UV. Using more lines reduces the systematic uncertainties in the determinations. Figure 8 highlights that it is still challenging to obtain a perfect fit for all lines of the same element, but the availability of more lines helps in identifying potential shortcomings in the atmosphere models. It also allows for a better determination of errors associated with abundance determinations, which is crucial for interpreting stellar evolution predictions of interior mixing. A full error determination will follow in a dedicated paper, but we could already say that typical error bars are 15–30%, sometimes up to 50%, with these two datasets combined (see Bouret et al. 2021), easily satisfying our science requirements.

Another key aspect of combining the ULLYSES and XShootU datasets is that it allows stellar and wind parameters

[5] The HST models are available at https://www.stsci.edu/hst/instrumentation/reference-data-for-calibration-and-tools/astronomical-catalogs/calspec.

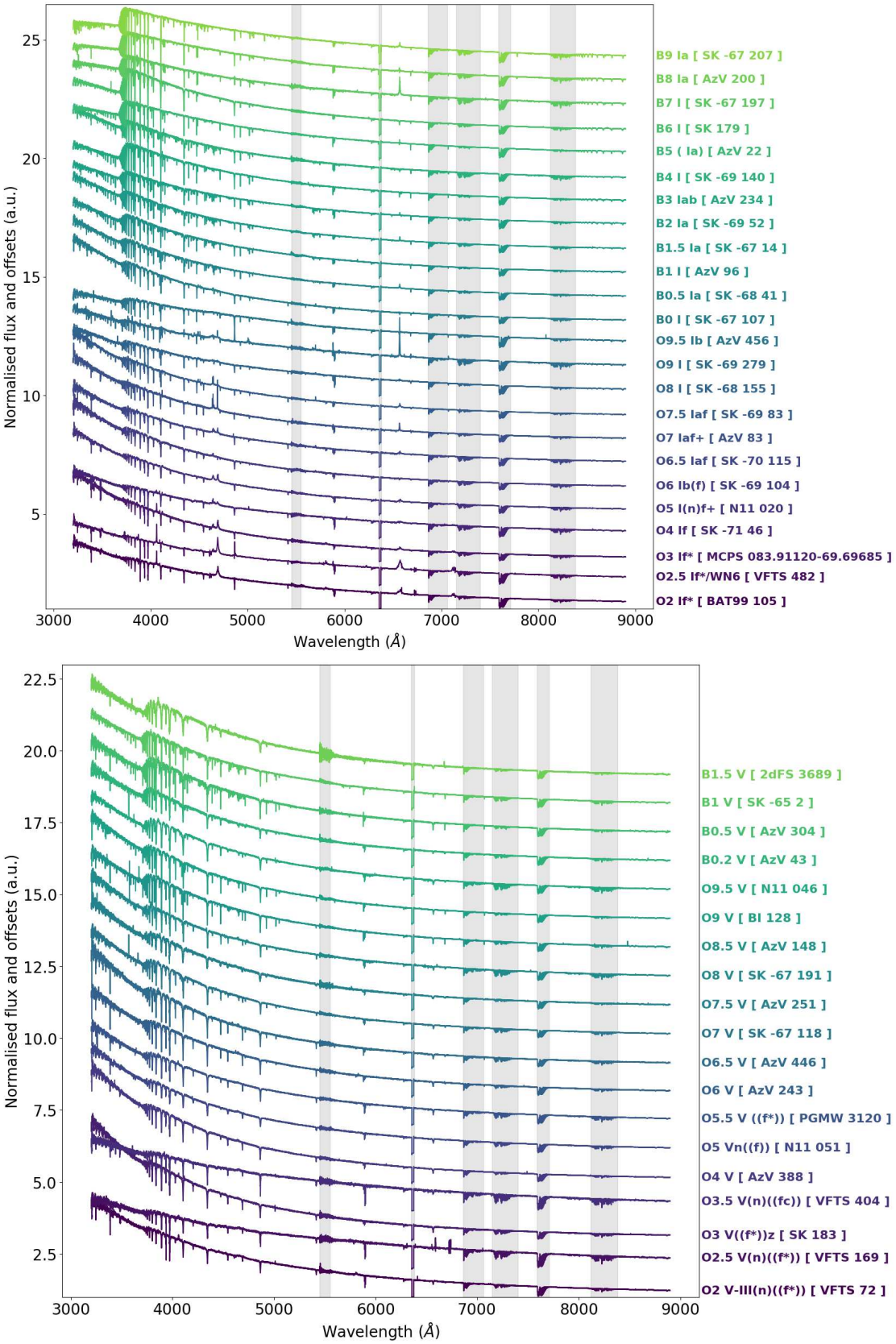

Fig. 6. Reduced X-shooter spectra for a range of spectral types of single-star supergiants (top) and dwarfs (bottom). For illustration purposes, the flux of each spectrum was divided by its mean value and an arbitrary offset was added. The grey regions correspond to the UVB-VIS common wavelength coverage (~5500 Å), a gap due to bad pixel masking (~6360 Å), and telluric absorption. Minor manual treatment to remove strong cosmic rays was performed.

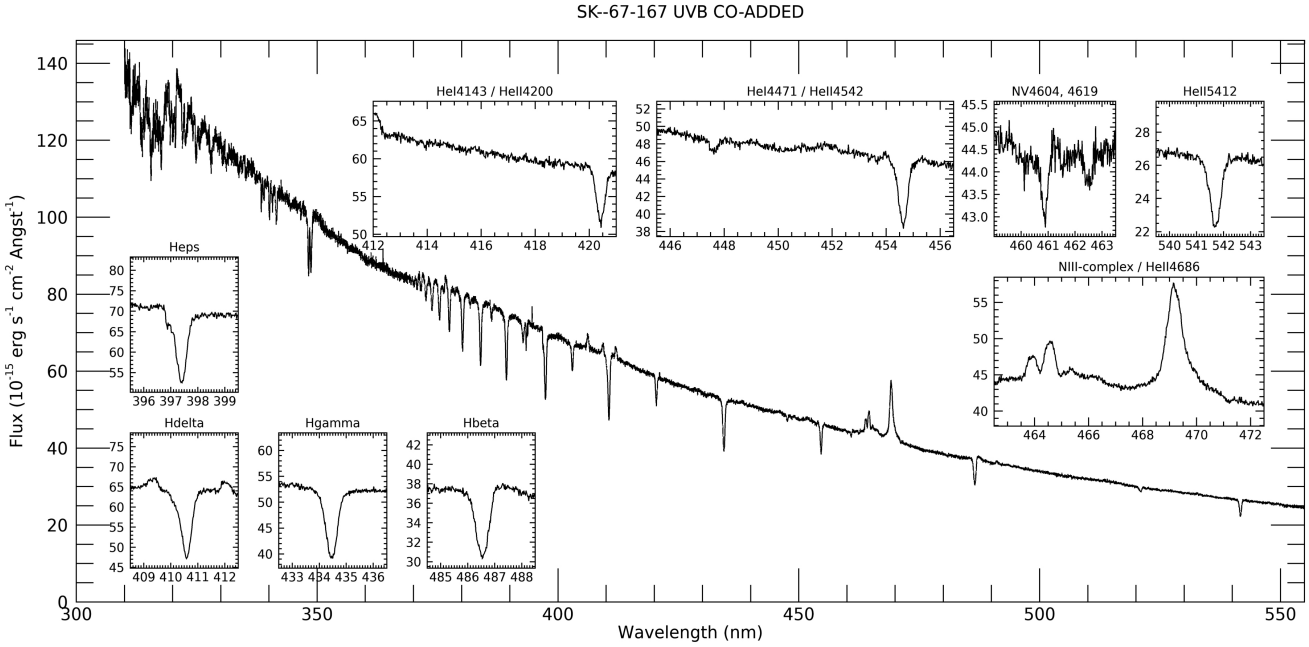

Fig. 7. X-shooter/UBV spectrum of Sk −67°167 (O4 Inf+) in the LMC, including zoomed-in views of key spectroscopic diagnostics.

to be derived self-consistently using both optical and UV diagnostics, which was lacking in surveys such as VFTS. For O-type stars, there are no conclusive diagnostics in the UV to derive effective temperatures and gravities. The wind profiles of O IV, O V, and N IV impose a minimum effective temperature, but they are also sensitive to the mass-loss rate and clumping properties. Figure 9 highlights which parameters can be determined from specific UV as well as optical lines for an LMC O supergiant.

As 30% of the sample involves B stars rather than O-type stars, we also show Fig. 10 highlighting which parameters can be determined from the UV versus optical part for B supergiants (Crowther et al. 2006; Firnstein & Przybilla 2012; McEvoy et al. 2015). The combination of UV and optical spectra is even more powerful for constraining the physical properties of B-type stars. As in the case of O-stars their UV spectrum alone does not contain diagnostics for gravity. Effective temperature could to first order be constrained by comparing the CII/CIII lines and the FeIII/FeIV line forests, although the C lines are also sensitive to mass loss, and Fe transitions depend also on $\log g$. The optical range offers cleaner $T_{\rm eff}$ diagnostics from the ionisation balance of SiII/SiIII/SiIV (secondarily, the comparison of HeI and MgII) and gravity (e.g. Hγ and the higher Balmer lines). The numerous metallic lines in the optical can be used to determine abundances and in the case of the strongest transitions (e.g. SiIII) micro-turbulence, and projected rotational velocity. The joint UV + optical range offers several mass-loss rate and clumping diagnostics, with the SiIV doublet being the best wind velocity indicator for early B supergiants.

In order to further quantify the need for optical X-shooter spectra in spectroscopic analyses, we present an example analysis for an O8 III SMC giant in Fig. 11. The figure shows both the UV part of the spectrum and some Hydrogen Balmer lines that are routinely utilised to derive $\log g$ values. It can easily be seen that while high and low $\log g$ model values reproduce the UV spectra equally well, the optical is critical for accurate $\log g$ determination. While the complexity of the spectroscopic analysis is beyond the scope of this paper, the key point is that UV-only fits yield very poorly constrained surface gravities, which result in enormous uncertainties on spectroscopic masses.

In addition to the uncertainty in surface gravity, it is also appropriate to mention that for stars with strong winds, such as supergiants, the Hα Balmer line is a key mass-loss and clumping factor diagnostic. When only accounting for micro-clumping and the UV part of the spectrum, Fullerton et al. (2006) showed that clumping factors were uncertain by factors of up to a hundred, and mass-loss rate reductions could easily be an order of magnitude. Only when accounting for the optical Hα line and macro-clumping (see Appendix A.4), Oskinova et al. (2007) showed that mass-loss rate uncertainties were significantly smaller, by a factor of 2 or so, and from the additional optical Hα line, clumping factors are usually estimated to be lower, of the order of 6–8 (e.g. Ramírez-Agudelo et al. 2017).

4.2. Spectroscopic analysis tools and procedures

XShootU is coordinating spectral modelling efforts for massive stars on a world-wide scale never witnessed before in the massive-star community. Before we can scale-up the analysis to hundreds of massive stars with hugely varying spectral and wind properties over the entire hot part of the HR diagram, it is paramount that codes and analysis techniques are tested and compared as a function of stellar parameters and metallicity.

The spectral analysis of massive stars is rather intricate due to the highly NLTE conditions in their turbulent, supersonic atmospheres. Over the past few decades, a number of highly complex, yet successful, model atmosphere codes have been developed, for example CMFGEN (Hillier & Miller 1998), PoWR (Hamann & Gräfener 2003; Sander et al. 2015), and FASTWIND (Santolaya-Rey et al. 1997; Puls et al. 2005). Although these codes have previously been applied to various sets of observations, only more recently have they been used for larger samples (e.g. Ramírez-Agudelo et al. 2017; Sabín-Sanjulián et al. 2017) due to the efficiency of numerical methods (applying certain physical approximations), and

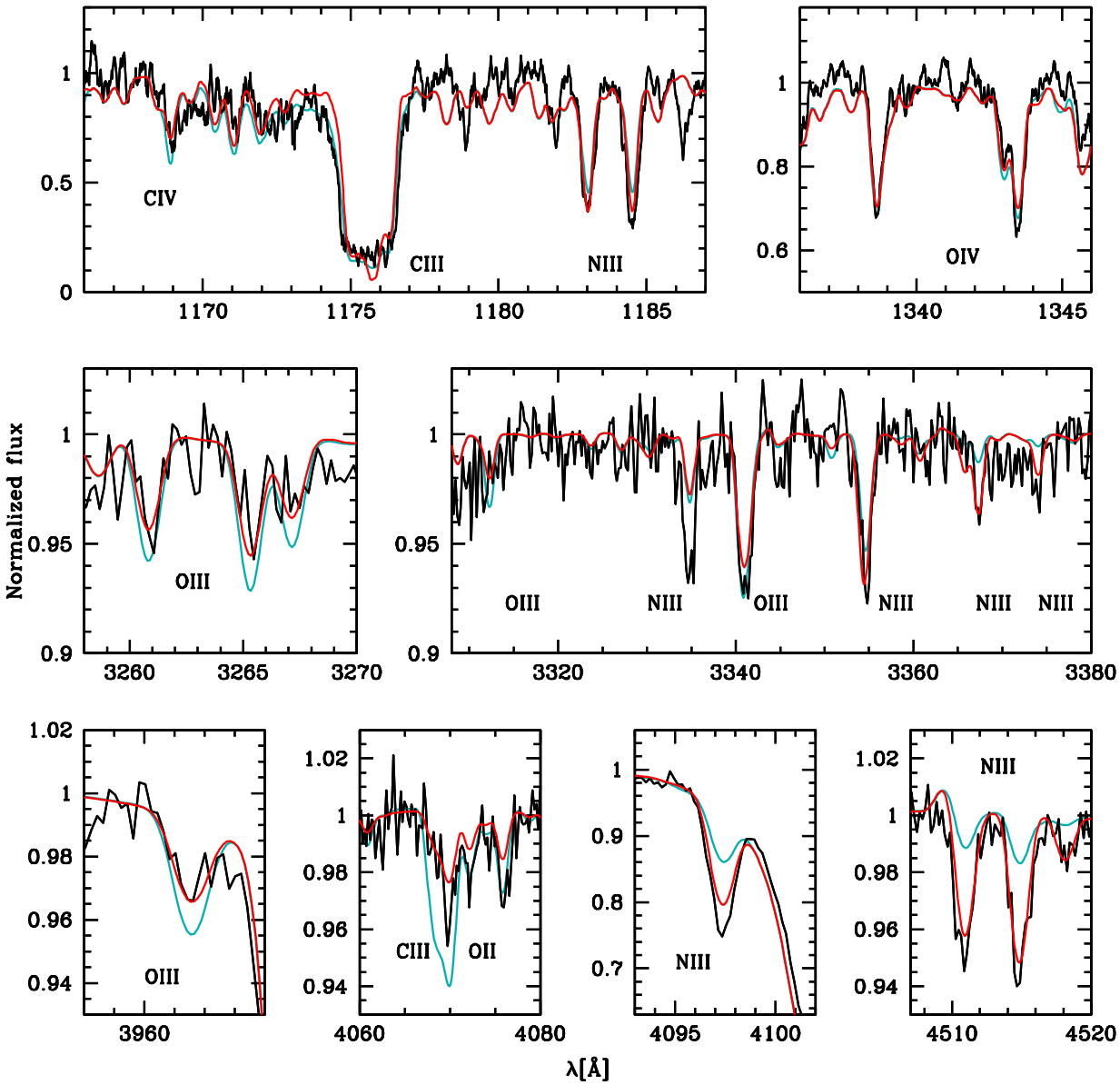

Fig. 8. Comparison between the observed HST (top) and X-shooter spectrum (black line) of selected lines of C, N, and O for AzV 327 (O9.5 II-Ibw) with two models (coloured lines). The light blue line is for solar-scaled abundances (factor of 1/5), while the red model has the following scaling: C abundance decreased by a factor of 3.8, N abundance increased by a factor of 4.5, and O abundance decreased by a factor of 1.6. The models were computed with the NLTE CMFGEN (Hillier & Miller 1998) atmosphere code.

efficient spectral automated analysis tools including genetic algorithms and grid-based χ^2 approaches.

At virtual and on-site Lorentz workshops in 2021 and 2022 (and various additional virtual XShootU meetings) preliminary comparisons of analyses with the various NLTE codes were performed by modelling subsets of O-stars. Agreement was reached on a common methodology for performing the spectroscopic analyses within the XShootU Project.

This recommended procedure is summarised as follows:

1. Use the same reference value for the distance moduli (DM) of the LMC and the SMC. We adopted DM(SMC) = 18.98 mag (Graczyk et al. 2020) and DM(LMC) = 18.48 mag (Pietrzyński et al. 2019).
2. Adopt the same photometry (U, B, V, J, H, K_S, as minimum) for each star (Table B.1). Optical photometry is from a variety of sources, whereas NIR photometry is from VISTA VMC (JKs; Cioni et al. 2011), 2MASS (JHKs; Cutri et al. 2003), or 2MASS 6X (JHKs; Cutri et al. 2012). H-band photometry is omitted if JKs values are discrepant between 2MASS and VMC owing to photometric variability or crowding.
3. Adopt the same literature source for the bolometric correction. The relation for bolometric correction as a function of $T_{\rm eff}$ and metallicity from Lanz & Hubeny (2003) is adopted for now. This relation may be updated in the course of this project.
4. Adopt the same reddening approach. Key references for the Milky Way foreground are Fitzpatrick et al. (2019), over earlier works by Seaton (1979), Cardelli et al. (1989), though Galactic foreground extinction is modest towards the Magellanic Clouds.

   For the Magellanic Cloud contributions, Gordon et al. (2003) is preferred, recognising earlier contributions from, for example, Howarth (1983) and Fitzpatrick (1986) to UV laws

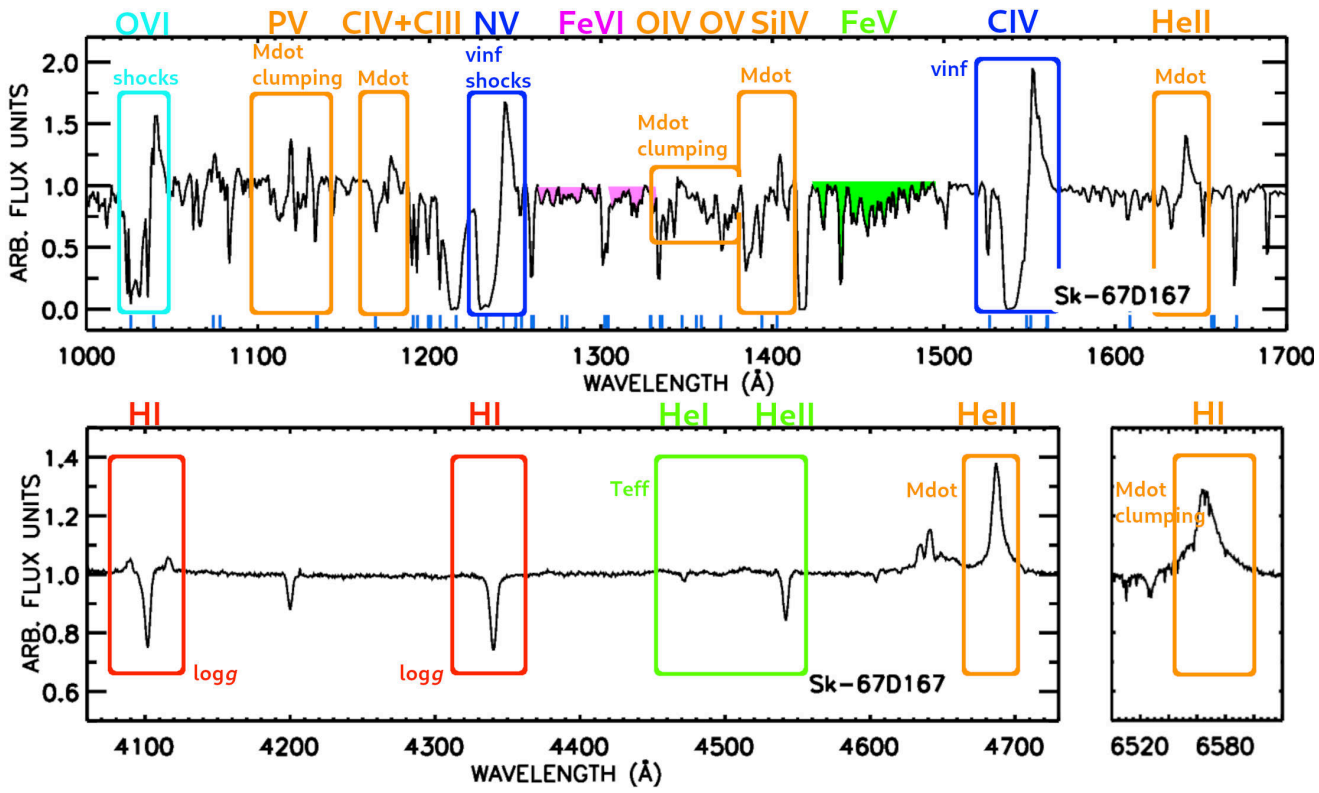

Fig. 9. UV (top) and optical (bottom) spectrum of the LMC star Sk-67 167 (O4 Inf+). The UV spectrum consists of STIS E140M observations taken as part of the ULLYSES project and archival FUSE data. The optical spectrum was obtained with X-shooter. A selection of diagnostics for stellar and wind parameters are highlighted. Note that these diagnostics can vary with spectral type. The ticks at the bottom of the UV spectra mark the position of interstellar lines.

in the LMC, and for the SMC from, for example, Prevot et al. (1984) and Bouchet et al. (1985) to the UV and optical/IR, respectively. For the FUSE range, Gordon et al. (2009) and Cartledge et al. (2005) are recommended for the Milky Way, and Magellanic Clouds, respectively.

5. Adopt the same baseline LMC and SMC abundances. Several abundance ratios in the Magellanic Clouds are notoriously non-solar, which is especially true for CNO in the SMC, and the use of scaled-solar values should be avoided when possible. Thus, the adopted abundance values were derived from an average of different determinations, for example from stars, H II regions, and SN remnants. The recommended values are listed in Tables 1 and 2. For several species, however, we need to agree on default abundances, given the absence of lines in spectral ranges covered by ULLYSES + XShootU. In such cases, scaled-solar values need to be adopted, using $0.5\,Z_\odot$ and $0.2\,Z_\odot$ scaling factors for the LMC and SMC, respectively (Asplund et al. 2009).
6. Whenever possible, adopt the same description of macro-turbulence for line broadening. The recommendation is to adopt a radial-tangential description of macro-turbulence (e.g. Simón-Díaz & Herrero 2014).
7. Adopt similar wind clumping implementation. We agreed to use the same parametric description as implemented in CMFGEN (Hillier & Miller 1998) for the standard derivation of the mass-loss rate. Clumping is predominately treated in the 'micro-clumping' approximation, assuming a void interclump medium. The volume filling factor, $f_{\rm V}$, has the following velocity-dependent behaviour:

$$f_{\rm V}(r) = f_{\rm V,\infty} + (1 - f_\infty)\, e^{-v(r)/v_{\rm cl}}, \quad (1)$$

where $f_{\rm V,\infty}$ denotes the value at $r \rightarrow \infty$. For a void interclump medium, the corresponding clumping factor $D \equiv f_{\rm cl}$ is simply the inverse value, implying that $D_\infty = f_{\rm V,\infty}^{-1}$. The free parameter $v_{\rm cl}$ is a characteristic velocity varied to describe the clumping onset. More sophisticated descriptions of the properties and nature of clumping can be implemented in the codes (e.g. Oskinova et al. 2007; Hawcroft et al. 2021; Flores & Hillier 2021). These predominately fall under the framework of working group (WG) 4 that focuses on wind structure (see below).

The next step is to benchmark the accuracy of stellar parameters derived with the different approaches. For this, a small set of stars was modelled with various NLTE codes. The obtained stellar parameters were compared, allowing us to assess to what extent the physical interpretation depends on the modelling tools applied. In parallel, we also considered bench-marking of the NLTE wind codes (i.e. against one another or against mock data) to perform a direct comparison of synthetic spectra computed for the same input model parameters. Alternatively, we could use a model obtained with one code and fit this model with the other codes. These various 'bench-marking' approaches will provide relevant information of systematic differences between codes, analyses tools, and other differences in approach, which will be detailed in a future (benchmarking) paper (Sander et al., in prep.; XShootU IV).

Determination of the wind terminal velocities (v_∞) is also taken on. As a global wind parameter, this is indeed an essential input for the models of stellar atmospheres used. The ULLYSES (UV) data are of particular importance for this task as they are rich in resonance transitions of ionised species, which are prime v_∞ diagnostics. For stars presenting saturated resonance-line

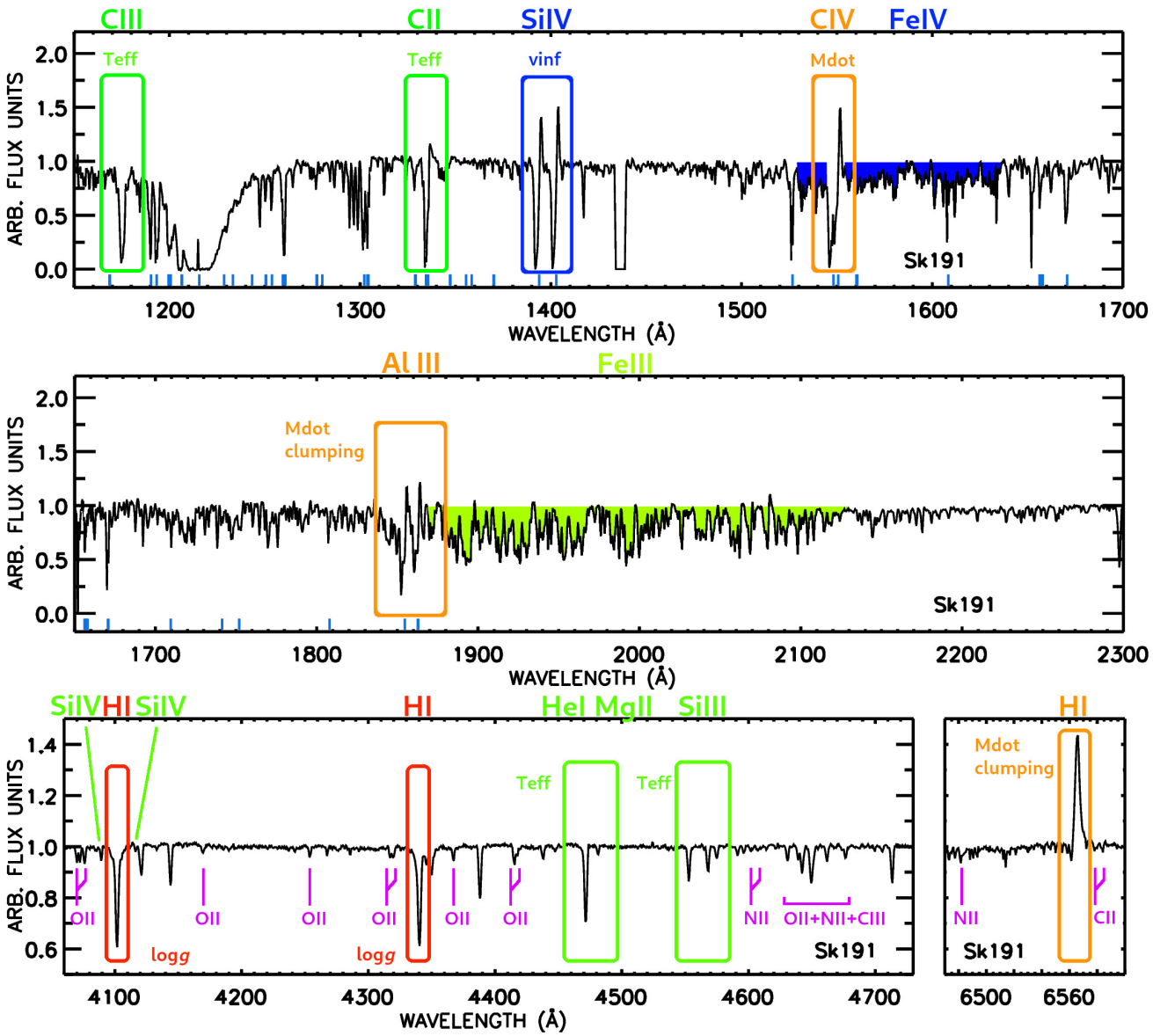

Fig. 10. UV (top, middle) and optical (bottom) spectrum of the SMC star Sk191 (B1.5 Ia). The UV spectrum consists of FUSE, STIS E140M, and STIS E230M observations compiled as part of the ULLYSES project. The optical spectrum was obtained with X-shooter. Similarly to Fig. 9, interstellar transitions and a selection of stellar and wind diagnostics are highlighted. In addition, metallic lines that can be used to measure abundances are marked in purple.

UV profiles, considering that the spectral lines remain optically thick at the distances where the wind reaches its maximum speed, v_∞ can be measured directly by measuring the maximum velocity shift of the absorption component of the UV C IV resonance doublet (see e.g. Prinja et al. 1990; Prinja & Crowther 1998). Alternatively, the wind speeds can also be measured by fitting synthetic spectra produced using the Sobolev with exact integration (SEI) method (Lamers et al. 1987). This latest approach is particularly relevant for stars without saturation in their UV resonance-line profile (although it can also be used in the first case mentioned above). As this paper is being written, a significant fraction of the LMC and SMC star sample has been studied with either method. Results concerning the dependence of v_∞ with the ambient metallicity or stellar parameters will be presented in dedicated papers (e.g. Hawcroft et al. 2023 XShootU III).

5. Final perspectives

The XShootU project is expected to provide many pieces of data, models, and new physics of massive stars in low-Z environments. It is important to stress that the overarching aim is to provide a high-quality homogeneous optical database that is complementary to ULLYSES. These legacy datasets are critical for a correct interpretation of unresolved high-Z observations with JWST/NIRSpec (Curti et al. 2023; Carnall et al. 2023; De Barros et al. 2019). The next goal is to provide uniformly determined stellar and wind parameters from the combined UV and optical datasets. For this part of the project, it is not only critical to include the correct NLTE physics, but also to test the various spectral synthesis codes and analyses.

A key science aim is to quantify "how" the mass-loss rate declines with decreasing metallicity. This does not

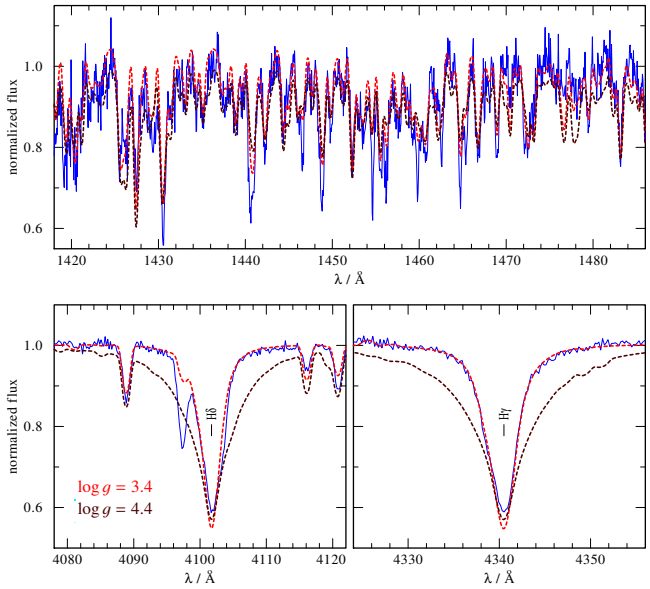

Fig. 11. O giant (AV186, O8.5III). The best fitting model is for $T = 33$ kK and $\log g = 3.4$. Note that while a ten times higher mass star with $\log g = 4.4$ would be indistinguishable in the UV, it would completely fail to reproduce the optical Balmer wings. The model was computed with the PoWR (Sander et al. 2017) NLTE code.

necessarily simply imply a determination of a power-law exponent, as the slope may easily vary with stellar parameters or Z itself (Vink et al. 2001; Kudritzki 2002; Sander & Vink 2020; Marcolino et al. 2022; Rickard et al. 2022). In order to obtain an empirical $\dot{M} = f(Z)$ relationship, we not only require mass-loss rates and clumping properties, but simultaneously also need to obtain the underlying stellar parameters ($T_{\rm eff}$, $\log g$, L, and M) as these parameters enable mass-loss properties from a given object in one galaxy to be compared to those from an entirely different object located elsewhere.

The XShootU dataset, coupled with surveys of H II regions in the LMC and SMC such as SDSS LVM[6] (Local Volume Mapper), represents a significant opportunity to advance the state-of-the-art in our understanding of how stars shape their environment. LVM is an optical (3600–10 000 Å) integral field unit (IFU) spectroscopic survey ($R \sim 4000$) of the Milky Way and the Local Group (LMC, SMC, M31, and M33). It will be the first IFU survey to isolate and resolve distinct environments within galaxies and to cover significant portions of the night sky. New population synthesis models – informed by the new physics obtained in the XShootU collaboration – can be used to remove the stellar contribution from LVM observations of star-forming regions, which will enable studies of the ionised gas alone (H II regions and diffuse ionised gas) over the large dynamic size range of LVM, from clusters and clouds (10–50 pc) to the kiloparsec scales of spiral arms, galactic inflows and outflows, and disk dynamics.

One should be aware that different communities refer to Z in different ways. Extra-galactic communities usually work on the basis of nebular oxygen (O) lines, while stellar astronomers are sometimes able to derive Fe abundances of individual stars. It is predominately the Fe abundance that sets the mass-loss rate, while intermediate mass elements such as O set the wind terminal velocity (Vink et al. 1999; Puls et al. 2000). While the [α/Fe] ratio in local dwarf galaxies such as IC 1613 is generally found to be sub-solar (Tautvaišienė et al. 2007; Garcia et al. 2014), Steidel et al. (2016) and Strom et al. (2022) show O to be enhanced in comparison to Fe for galaxies at intermediate redshifts ('Cosmic Noon'). This is thought to be due to the time delay in the production of Fe from Type Ia SNe with respect to α elements released by massive stars. It may therefore become relevant to consider more detailed abundance patterns than simply scaling all metals with the solar-abundance pattern, that is, to make a clearer distinction between [Fe/H] and α elements for $\dot{M}$ calibrations of massive stars, as indicated in Table 5 of Vink et al. (2001). The ULLYSES and XShootU sample will uniquely provide the opportunity to investigate potential differences between [Fe/H] and α elements with non-solar patterns.

When we are eventually able to provide a reliable empirical $\dot{M} = f(Z)$ relation, we will be able to compare these findings to theoretical predictions, and this will inform us on how to treat mass loss more reliably in models of stellar evolution – and thereby also in feedback and population synthesis studies – at low Z. It is currently unclear if most of the mass loss takes place in Z-dependent winds, or in Z-independent eruptions or binary interactions. Despite the possibility of significant Z-independent mass loss, there is ample evidence that massive-star evolution in metal-poor environments proceeds very differently from such evolution in our Milky Way. Shirazi & Brinchmann (2012) and Kehrig et al. (2015) found strong nebular He II emission lines in low-Z galaxies, but not in metal-rich ones. Long-duration gamma-ray bursts (e.g. Vreeswijk et al. 2004), super-luminous SNe (e.g. Quimby et al. 2011; Gal-Yam 2012; Chen et al. 2015), and broad-line Type Ic SNe occur preferentially in low-Z dwarf galaxies (e.g. Palmerio et al. 2019),whereas ordinary Type Ic SNe avoid dwarf galaxies.

The spectacular merger of two ~30 $M_\odot$ BHs observed through the detection of GWs by the LIGO observatory (Abbott et al. 2016a) most likely originated from a system that had an initial Z similar to that of the SMC (Abbott et al. 2016b). This conclusion is inextricably linked to the predicted reduced stellar wind mass loss at low Z (e.g. Vink et al. 2001). Proposed channels that may have led to GW 150914 (and other more recent events) involve mass transfer and common envelope evolution (e.g. Belczynski et al. 2016) and CHE systems (Mandel & de Mink 2016). The CHE model is linked to rapid spin rates, leading to rotationally induced mixing of the stellar interior (Maeder 1987; Yoon & Langer 2005). Predictions of single star evolution have shown this process to be increasingly important at lower Z (Brott et al. 2011) due to lower mass-loss rates, and correspondingly less angular momentum loss. Support for the existence of CHE can be found in the properties of a small fraction of WR stars (Martins et al. 2009; Hainich et al. 2015), but CHE still lacks unambiguous observational confirmation in the O-star regime (see for example Walborn et al. 2004; Abdul-Masih et al. 2019, 2021 and Bouret et al. 2013 for candidates).

The properties of GW events and exotic SNe illustrate the key physics involved: spin rates and rotationally induced mixing, CHE, and wind mass-loss rates. The XShootU sample consists of uniformly estimated spectral parameters of objects previously classified in the literature to varying extents. Further analysis will include, for instance, a determination of an upper limit to the number of CHE stars for which three basic observables need to be fulfilled: (i) a peculiar HR diagram location, as chemically homogeneous stars evolve bluewards instead of redwards, (ii) higher average $v \sin i$, as they are thought to be caused by rapid rotation, and (iii) special chemical-abundance patterns that showcase chemical mixing.

These are just some of the studies that are being prepared, and their results will be published in research articles of the

[6] https://www.sdss.org/dr18/lvm/about/

Table 1. Baseline LMC metal abundances (X/H by number) with respect to $Z_\odot$ from Magg et al. (2022, MBS22).

Element	SNR	H II regions				B stars			F supergiants		⟨LMC⟩	Solar	⟨LMC⟩	
	D19	G99	P03/SCT17	T03	L08	K00/K05	T07/H07	D18	HAS95	A01	X/H	MBS22	log X/H + 12	$Z_\odot$
C	1.2×10^{-4}	7.9×10^{-5}	1.0×10^{-4}	···	···	9.5×10^{-5}	···	···	1.2×10^{-4}	8.9×10^{-5}	1.0×10^{-4}	3.6×10^{-4}	8.01	0.28
N	(1.6×10^{-5})	7.9×10^{-6}	1.6×10^{-5}	···	···	1.0×10^{-5}	7.9×10^{-6}	···	···	···	1.1×10^{-5}	9.5×10^{-5}	7.03	0.12
O	2.2×10^{-4}	2.5×10^{-5}	3.2×10^{-4}	2.2×10^{-4}	···	2.5×10^{-4}	2.3×10^{-4}	···	(2.8×10^{-4})	(3.2×10^{-4})	2.5×10^{-4}	5.9×10^{-4}	8.40	0.42
Ne	4.0×10^{-5}	4.0×10^{-5}	6.8×10^{-5}	4.6×10^{-5}	5.8×10^{-5}	···	···	···	···	···	5.0×10^{-5}	1.4×10^{-4}	7.70	0.35
Na	···	···	···	···	···	···	···	···	1.5×10^{-6}	7.9×10^{-7}	1.2×10^{-6}	1.9×10^{-6}	6.1	0.6
Mg	1.5×10^{-5}	···	···	···	···	1.4×10^{-5}	1.2×10^{-5}	1.0×10^{-5}	1.6×10^{-5}	···	1.3×10^{-5}	3.5×10^{-5}	7.13	0.46
Al	···	···	···	···	···	7.2×10^{-7}	···	···	2.2×10^{-6}	···	1.5×10^{-6}	2.7×10^{-6}	6.2	0.5
Si	1.3×10^{-5}	5.0×10^{-6}	···	···	···	1.2×10^{-5}	1.6×10^{-5}	···	(3.7×10^{-5})	···	1.1×10^{-5}	3.9×10^{-5}	7.06	0.32
S	9.5×10^{-6}	5.0×10^{-6}	9.8×10^{-6}	5.9×10^{-6}	5.9×10^{-6}	···	···	···	9.9×10^{-6}	···	7.7×10^{-6}	1.4×10^{-5}	6.88	0.53
Cl	9.1×10^{-8}	···	6.6×10^{-8}	···	···	···	···	···	···	···	7.9×10^{-8}	1.8×10^{-7}	4.9	0.4
Ar	6.2×10^{-7}	1.6×10^{-6}	1.8×10^{-6}	1.4×10^{-6}	2.1×10^{-6}	···	···	···	···	···	1.5×10^{-6}	3.2×10^{-6}	6.2	0.5
Ca	1.0×10^{-6}	···	···	···	···	···	···	···	1.6×10^{-6}	···	1.3×10^{-6}	2.3×10^{-6}	6.1	0.6
Cr	2.2×10^{-7}	···	···	···	···	···	···	···	2.6×10^{-7}	···	2.4×10^{-7}	5.5×10^{-7}	5.4	0.4
Fe	2.1×10^{-5}	···	(2.5×10^{-6})	···	(1.7×10^{-6})	1.2×10^{-5}	1.7×10^{-5}	···	1.7×10^{-5}	···	1.7×10^{-5}	3.2×10^{-5}	7.23	0.54
Ni	7.9×10^{-7}	···	···	···	···	···	···	···	9.2×10^{-7}	···	8.6×10^{-7}	1.7×10^{-6}	5.9	0.5

Notes. Values shown in parentheses are excluded from the average, due to issues with enhancements owing to mixing (e.g. N), depletion on dust grains (Fe) or other concerns. log(P/H) + 12 = 5.1 or 0.5 $Z_\odot$ is adopted for P following ISM studies of Tchernyshyov et al. (2015).
References. HAS95: Hill et al. (1995); G99: Garnett (1999); K00: Korn et al. (2000; He/Al/Fe only); K05: Korn et al. (2005; excl He/Al/Fe); A01: Andrievsky et al. (2001); P03: Peimbert et al. (2019; excl. C/O); T03: Tsamis et al. (2003); T07: Trundle et al. (2007); H07: Hunter et al. (2007); L08: Lebouteiller et al. (2008); SCT17: Toribio San Cipriano et al. (2017; C/O recomb lines for 30 Dor); D18: Dufton et al. (2018); D19: Dopita et al. (2019).

Table 2. Baseline SMC metal abundances (X/H by number) adopted with respect to $Z_\odot$ from Magg et al. (2022, MBS22).

Element	SNR	H II regions				A stars	B stars		K supergiants		⟨SMC⟩	Solar	⟨SMC⟩	
	D19	KD98	G99	R02	L08	V99	K00	T07/H09	H97/HBS97	H99	X/H	MBS22	log X/H + 12	$Z_\odot$
C	3.2×10^{-5}	1.6×10^{-5}	2.5×10^{-5}	···	···	···	2.5×10^{-5}	2.0×10^{-5}	3.6×10^{-5}	2.8×10^{-5}	2.6×10^{-5}	3.6×10^{-4}	7.42	0.07
N	6.6×10^{-6}	3.6×10^{-6}	3.2×10^{-6}	6.5×10^{-6}	···	(2.1×10^{-5})	3.2×10^{-6}	(1.7×10^{-5})	(3.2×10^{-5})	···	4.6×10^{-6}	9.5×10^{-5}	6.66	0.05
O	1.0×10^{-4}	1.0×10^{-4}	1.0×10^{-4}	1.4×10^{-4}	···	1.4×10^{-4}	1.4×10^{-4}	9.8×10^{-5}	1.2×10^{-4}	···	1.1×10^{-4}	5.9×10^{-4}	8.05	0.19
Ne	1.1×10^{-5}	1.6×10^{-5}	1.6×10^{-5}	2.1×10^{-5}	2.2×10^{-5}	···	···	···	2.9×10^{-5}	···	1.7×10^{-5}	1.4×10^{-4}	7.23	0.12
Na	···	···		···.	···	···	···	···	4.0×10^{-7}	2.6×10^{-7}	3.1×10^{-7}	1.9×10^{-6}	5.49	0.16
Mg	5.2×10^{-6}	···	···	···	···.	6.7×10^{-6}	6.0×10^{-6}	5.2×10^{-6}	1.1×10^{-5}	4.5×10^{-6}	6.1×10^{-6}	3.5×10^{-5}	6.78	0.17
Al	···	···	···	···	···	···	3.8×10^{-7}	···	4.6×10^{-7}	3.6×10^{-7}	3.9×10^{-7}	2.7×10^{-6}	5.59	0.15
Si	5.9×10^{-6}	···	2.0×10^{-6}	···	···	9.3×10^{-6}	6.9×10^{-6}	5.9×10^{-6}	5.2×10^{-6}	5.6×10^{-6}	5.3×10^{-6}	3.9×10^{-5}	6.72	0.14
S	···	···	2.0×10^{-6}	2.5×10^{-6}	2.3×10^{-6}	···	···	···	···.	···	2.3×10^{-6}	1.4×10^{-5}	6.36	0.16
Cl	2.3×10^{-8}	···.	···	···	···	···	···	···	···	···	2.3×10^{-8}	1.8×10^{-7}	4.37	0.13
Ar	5.1×10^{-7}	···	7.9×10^{-7}	6.6×10^{-7}	9.3×10^{-7}	···	···	···	···	···	7.2×10^{-7}	3.2×10^{-6}	5.86	0.23
Ca	5.9×10^{-7}	···	···	···	···	2.1×10^{-7}	···	···	3.9×10^{-7}	3.3×10^{-7}	4.1×10^{-7}	2.3×10^{-6}	5.61	0.17
Cr	···	···	···	···	···	···	···	···	4.6×10^{-8}	3.7×10^{-8}	4.0×10^{-8}	5.5×10^{-7}	4.61	0.07
Fe	5.9×10^{-6}	···	···	···	···	5.1×10^{-6}	6.6×10^{-6}	8.5×10^{-6}	6.4×10^{-6}	5.1×10^{-6}	6.3×10^{-6}	3.2×10^{-5}	6.80	0.20
Ni	3.5×10^{-7}	···	···	···	···	···	···	···	3.4×10^{-7}	1.2×10^{-7}	2.4×10^{-7}	1.7×10^{-6}	5.37	0.14

Notes. Values shown in parentheses are excluded from the average, due to issues with enhancements owing to mixing (e.g. N), depletion on dust grains (Fe) or other concerns. log(P/H) + 12 = 4.7 or 0.2 $Z_\odot$ is adopted for P from ISM studies of Tchernyshyov et al. (2015).
References. H97: Hill (1997); HBS97: Hill et al. (1997); KD98: Kurt et al. (1998); G99: Garnett (1999); V99: Venn (1999); H99: Hill (1999); K00: Korn et al. (2000); T07: Trundle et al. (2007); L08: Lebouteiller et al. (2008); H09: Hunter et al. (2009); D19: Dopita et al. (2019).

XShootU series. It should be emphasised that some of the analysis is already ongoing, but there is ample space for new parties to join the project. Moreover, the X-shooter data are open to the public, and we also plan to make the higher level data products open to the community at large, as these high-quality data have long-term utility for research projects that may not yet be foreseen.

Acknowledgements. We thank the ESO support staff for the help in the preparation of the observations, in the scheduling, and for carrying out the observations at Paranal. We also thank the ESO support staff, in particular Carlo Felice Manara. We also thank the ULLYSES teams at STScI, in particular, Julia Roman-Duval and STScI Director Ken Sembach, for executing and enabling the ULLYSES Director's Discretionary program. Based on observations obtained with the NASA/ESA *Hubble* Space Telescope, retrieved from the Mikulski Archive for Space Telescopes (MAST) at the Space Telescope Science Institute (STScI). STScI is operated by the Association of Universities for Research in Astronomy, Inc. under NASA contract NAS 5-26555. JSV and ERH gratefully acknowledge support from STFC via grant ST/V000233/1. LPM thanks CNPQ for financial support through grant 307115/2021-6. AW acknowledges the support of UNAM via grant agreement PAPIIT no. IN106922. ADU acknowledges support from NASA under award number 80GSFC21M0002. DMB gratefully acknowledges funding from the Research Foundation Flanders (FWO) by means of a senior postdoctoral fellowship with grant agreement number 1286521N. AACS acknowledges support by the Deutsche Forschungsgemeinschaft (DFG - German Research Foundation) in the form of an Emmy Noether Research Group – Project-ID 445674056 (SA4064/1-1, PI Sander). BK gratefully acknowledges support from the Grant Agency of the Czech Republic (GAČR 22-34467S). The Astronomical Institute in Ondřejov is supported by the project RVO:67985815. CJE gratefully acknowledges support for this work provided by NASA through grant number HST-AR-15794.001-A from the Space Telescope Science Institute, which is operated by AURA, Inc., under NASA contract NAS 5-26555. NSL wishes to thank the National Sciences and Engineering Council of Canada (NSERC) for financial support. AuD acknowledges support by NASA through *Chandra* Award number TM1-22001B and GO2-23003X issued by the *Chandra* X-ray Observatory 27 Center, which is operated by the Smithsonian Astrophysical Observatory for and on behalf of NASA under contract NAS8-03060. In addition, AuD acknowledges NASA ATP grant number 80NSSC22K0628. GM acknowledges funding support from the EuŁropean Research Council (ERC) under the European Union's

Horizon 2020 research and innovation programme (Grant agreement No. 772086). RI gratefully acknowledges support by the National Science Foundation under Grant No. AST-2009412. JMA acknowledges support from the Spanish Government Ministerio de Ciencia e Innovación through grant PGC2018-095 049-B-C22. CJKL gratefully acknowledges support from the International Max Planck Research School for Astronomy and Cosmic Physics at the University of Heidelberg in the form of an IMPRS PhD fellowship. NDK acknowledges support from the National Solar Observatory, which is managed by the Association of Universities for Research in Astronomy, Inc. and funded by the National Science Foundation. MG and FN gratefully acknowledge funding by grants PID2019-105552RB-C41 and MDM-2017-0737 Unidad de Excelencia "María de Maeztu"-Centro de Astrobiología (INTA-CSIC) by the Spanish Ministry of Science and Innovation/State Agency of Research MCIN/AEI/10.13039/501100011033 and by "ERDF A way of making Europe". We thank the Lorentz Centre in Leiden for hosting "ULLYSES sets sail: massive star spectroscopy with HST and the ESO VLT".

References

Abbott, B. P., Abbott, R., Abbott, T. D., et al. 2016a, Phys. Rev. Lett., 116, 241102
Abbott, B. P., Abbott, R., Abbott, T. D., et al. 2016b, ApJ, 818, L22
Abbott, B. P., Abbott, R., Abbott, T. D., & Abraham, S. 2020, ApJ, 892, L3
Abdul-Masih, M., Sana, H., Sundqvist, J., et al. 2019, ApJ, 880, 115
Abdul-Masih, M., Sana, H., Hawcroft, C., et al. 2021, A&A, 651, A96
Aerts, C., Thoul, A., Daszyńska, J., et al. 2003, Science, 300, 1926
Alcock, C., Allsman, R. A., Alves, D., et al. 1997, AJ, 114, 326
Andrievsky, S. M., Kovtyukh, V. V., Korotin, S. A., Spite, M., & Spite, F. 2001, A&A, 367, 605
Ardeberg, A. 1980, A&AS, 42, 1
Ardeberg, A., & Maurice, E. 1977, A&AS, 30, 261
Ardeberg, A., Brunet, J. P., Maurice, E., & Prevot, L. 1972, A&AS, 6, 249
Asplund, M., Grevesse, N., Sauval, A. J., & Scott, P. 2009, ARA&A, 47, 481
Azzopardi, M., & Vigneau, J. 1982, A&AS, 50, 291
Azzopardi, M., Vigneau, J., & Macquet, M. 1975, A&AS, 22, 285
Bailey, M., van Loon, J. T., Sarre, P. J., & Beckman, J. E. 2015, MNRAS, 454, 4013
Belczynski, K., Bulik, T., Fryer, C. L., et al. 2010, ApJ, 714, 1217
Belczynski, K., Holz, D. E., Bulik, T., & O'Shaughnessy, R. 2016, Nature, 534, 512
Bell, S. A., Hill, G., Hilditch, R. W., et al. 1991, MNRAS, 250, 119
Berg, D. A., James, B. L., King, T., et al. 2022, ApJS, 261, 31
Bestenlehner, J. M., Gräfener, G., Vink, J. S., et al. 2014, A&A, 570, A38
Björklund, R., Sundqvist, J. O., Puls, J., & Najarro, F. 2021, A&A, 648, A36
Blair, W. P., Oliveira, C., LaMassa, S., et al. 2009, PASP, 121, 634
Bohlin, R. C., Hubeny, I., & Rauch, T. 2020, AJ, 160, 21
Bonnarel, F., Fernique, P., Bienaymé, O., et al. 2000, A&AS, 143, 33
Bouchet, P., Lequeux, J., Maurice, E., Prevot, L., & Prevot-Burnichon, M. L. 1985, A&A, 149, 330
Bouret, J. C., Lanz, T., Hillier, D. J., et al. 2003, ApJ, 595, 1182
Bouret, J. C., Lanz, T., Martins, F., et al. 2013, A&A, 555, A1
Bouret, J. C., Martins, F., Hillier, D. J., et al. 2021, A&A, 647, A134
Bowman, D. M. 2020, Front. Astron. Space Sci., 7, 70
Bowman, D. M., Burssens, S., Pedersen, M. G., et al. 2019, Nat. Astron., 3, 760
Brands, S. A., de Koter, A., Bestenlehner, J. M., et al. 2022, A&A, 663, A36
Brott, I., de Mink, S. E., Cantiello, M., et al. 2011, A&A, 530, A115
Burssens, S., Simón-Díaz, S., Bowman, D. M., et al. 2020, A&A, 639, A81
Buscombe, W., & Foster, B. E. 1995, MK Spectral Classifications. Twelfth General Catalogue, Epoch 2000 Including UBV Photometry
Cardelli, J. A., Clayton, G. C., & Mathis, J. S. 1989, ApJ, 345, 245
Carnall, A. C., Begley, R., McLeod, D. J., et al. 2023, MNRAS, 518, L45
Cartledge, S. I. B., Clayton, G. C., Gordon, K. D., et al. 2005, ApJ, 630, 355
Castro, N., Oey, M. S., Fossati, L., & Langer, N. 2018, ApJ, 868, 57
Chen, T. W., Smartt, S. J., Jerkstrand, A., et al. 2015, MNRAS, 452, 1567
Cioni, M. R. L., Clementini, G., Girardi, L., et al. 2011, A&A, 527, A116
Conti, P. S., Garmany, C. D., & Massey, P. 1986, AJ, 92, 48
Cox, N. L. J., Cordiner, M. A., Cami, J., et al. 2006, A&A, 447, 991
Cox, N. L. J., Cordiner, M. A., Ehrenfreund, P., et al. 2007, A&A, 470, 941
Crampton, D., & Greasley, J. 1982, PASP, 94, 31
Crowther, P. A., & Smith, L. J. 1997, A&A, 320, 500
Crowther, P. A., & Walborn, N. R. 2011, MNRAS, 416, 1311
Crowther, P. A., Dessart, L., Hillier, D. J., Abbott, J. B., & Fullerton, A. W. 2002a, A&A, 392, 653
Crowther, P. A., Hillier, D. J., Evans, C. J., et al. 2002b, ApJ, 579, 774
Crowther, P. A., Lennon, D. J., & Walborn, N. R. 2006, A&A, 446, 279
Cutri, R. M., Skrutskie, M. F., van Dyk, S., et al. 2003, VizieR Online Data Catalog: II/246
Cutri, R. M., Skrutskie, M. F., van Dyk, S., et al. 2012, VizieR Online Data Catalog: II/281
Curti, M., D'Eugenio, F., Carniani, S., et al. 2023, MNRAS, 518, 425
David-Uraz, A., Neiner, C., Sikora, J., et al. 2019, MNRAS, 487, 304
De Barros, S., Oesch, P. A., Labbé, I., et al. 2019, MNRAS, 489, 2355
Dopita, M. A., Seitenzahl, I. R., Sutherland, R. S., et al. 2019, AJ, 157, 50
Doran, E. I., Crowther, P. A., de Koter, A., et al. 2013, A&A, 558, A134
Dufton, P. L., Ryans, R. S. I., Trundle, C., et al. 2005, A&A, 434, 1125
Dufton, P. L., Ryans, R. S. I., Simón-Díaz, S., Trundle, C., & Lennon, D. J. 2006, A&A, 451, 603
Dufton, P. L., Thompson, A., Crowther, P. A., et al. 2018, A&A, 615, A101
Dufton, P. L., Evans, C. J., Hunter, I., Lennon, D. J., & Schneider, F. R. N. 2019, A&A, 626, A50
Dupret, M. A., Thoul, A., Scuflaire, R., et al. 2004, A&A, 415, 251
Ehrenfreund, P., Cami, J., Jiménez-Vicente, J., et al. 2002, ApJ, 576, L117
Ekström, S., Georgy, C., Eggenberger, P., et al. 2012, A&A, 537, A146
Erba, C., David-Uraz, A., Petit, V., et al. 2021, MNRAS, 506, 5373
Evans, C. J., Crowther, P. A., Fullerton, A. W., & Hillier, D. J. 2004a, ApJ, 610, 1021
Evans, C. J., Howarth, I. D., Irwin, M. J., Burnley, A. W., & Harries, T. J. 2004b, MNRAS, 353, 601
Evans, C. J., Lennon, D. J., Trundle, C., Heap, S. R., & Lindler, D. J. 2004c, ApJ, 607, 451
Evans, C. J., Lennon, D. J., Smartt, S. J., & Trundle, C. 2006, A&A, 456, 623
Evans, C. J., Bresolin, F., Urbaneja, M. A., et al. 2007, ApJ, 659, 1198
Evans, C. J., Taylor, W. D., Hénault-Brunet, V., et al. 2011, A&A, 530, A108
Evans, C. J., Kennedy, M. B., Dufton, P. L., et al. 2015a, A&A, 574, A13
Evans, C. J., van Loon, J. T., Hainich, R., & Bailey, M. 2015b, A&A, 584, A5
Fariña, C., Bosch, G. L., Morrell, N. I., Barbá, R. H., & Walborn, N. R. 2009, AJ, 138, 510
Feitzinger, J. V., & Isserstedt, J. 1983, A&AS, 51, 505
Ferland, G. J., Chatzikos, M., Guzmán, F., et al. 2017, Rev. Mex. Astron. Astrofis., 53, 385
Firnstein, M., & Przybilla, N. 2012, A&A, 543, A80
Fitzgerald, M. P. 1970, A&A, 4, 234
Fitzpatrick, E. L. 1986, AJ, 92, 1068
Fitzpatrick, E. L. 1988, ApJ, 335, 703
Fitzpatrick, E. L. 1991, PASP, 103, 1123
Fitzpatrick, E. L., Massa, D., Gordon, K. D., Bohlin, R., & Clayton, G. C. 2019, ApJ, 886, 108
Flores, B. L., & Hillier, D. J. 2021, MNRAS, 504, 311
Foellmi, C., Moffat, A. F. J., & Guerrero, M. A. 2003, MNRAS, 338, 360
Fullerton, A. W., Massa, D. L., & Prinja, R. K. 2006, ApJ, 637, 1025
Gal-Yam, A. 2012, Science, 337, 927
Garcia, M., Herrero, A., Najarro, F., Lennon, D. J., & Alejandro Urbaneja, M. 2014, ApJ, 788, 64
Garcia, M., Herrero, A., Najarro, F., Camacho, I., & Lorenzo, M. 2019, MNRAS, 484, 422
Garland, R., Dufton, P. L., Evans, C. J., et al. 2017, A&A, 603, A91
Garmany, C. D., & Walborn, N. R. 1987, PASP, 99, 240
Garmany, C. D., Conti, P. S., & Massey, P. 1987, AJ, 93, 1070
Garmany, C. D., Massey, P., & Parker, J. W. 1994, AJ, 108, 1256
Garnett, D. R. 1999, in New Views of the Magellanic Clouds, eds. Y. H. Chu, N. Suntzeff, J. Hesser, & D. Bohlender, 190, 266
Goldoni, P. 2011, Astron. Nachr., 332, 227
Gordon, K. D., Clayton, G. C., Misselt, K. A., Landolt, A. U., & Wolff, M. J. 2003, ApJ, 594, 279
Gordon, K. D., Cartledge, S., & Clayton, G. C. 2009, ApJ, 705, 1320
Götberg, Y., de Mink, S. E., Groh, J. H., et al. 2018, A&A, 615, A78
Graczyk, D., Soszyński, I., Poleski, R., et al. 2011, Acta Astron., 61, 103
Graczyk, D., Pietrzyński, G., Thompson, I. B., et al. 2020, ApJ, 904, 13
Gräfener, G., Koesterke, L., & Hamann, W. R. 2002, A&A, 387, 244
Grin, N. J., Ramírez-Agudelo, O. H., de Koter, A., et al. 2017, A&A, 600, A82
Groh, J. H., Meynet, G., Ekström, S., & Georgy, C. 2014, A&A, 564, A30
Grunhut, J. H., Wade, G. A., Neiner, C., et al. 2017, MNRAS, 465, 2432
Gvaramadze, V. V., Kniazev, A. Y., Maryeva, O. V., & Berdnikov, L. N. 2018, MNRAS, 474, 1412
Haefner, R., Simon, K. P., & Fiedler, A. 1994, A&A, 288, L9
Hainich, R., Rühling, U., Todt, H., et al. 2014, A&A, 565, A27
Hainich, R., Pasemann, D., Todt, H., et al. 2015, A&A, 581, A21
Hamann, W. R., & Gräfener, G. 2003, A&A, 410, 993
Hamann, W. R., Feldmeier, A., & Oskinova, L. M. 2008, Clumping in hot-star winds: Proc. International Workshop held in Potsdam, Germany, 18-22 June 2007, eds. W.-R. Hamann, A. Feldmeier, & L. M. Oskinova
Hawcroft, C., Sana, H., Mahy, L., et al. 2021, A&A, 655, A67
Hawcroft, C., Sana, H., Mahy, L., et al. 2023, A&A in press https://doi.org/10.1051/0004-6361/202245588
Heap, S. R., Lanz, T., & Hubeny, I. 2006, ApJ, 638, 409
Herrero, A., Kudritzki, R. P., Vilchez, J. M., et al. 1992, A&A, 261, 209
Heydari-Malayeri, M., & Hutsemekers, D. 1991, A&A, 243, 401

Hill, V. 1997, A&A, 324, 435
Hill, V. 1999, A&A, 345, 430
Hill, V., Andrievsky, S., & Spite, M. 1995, A&A, 293, 347
Hill, V., Barbuy, B., & Spite, M. 1997, A&A, 323, 461
Hillier, D. J. 2020, Galaxies, 8, 60
Hillier, D. J., & Miller, D. L. 1998, ApJ, 496, 407
Hosek, Jr., M. W., Kudritzki, R. P., Bresolin, F., et al. 2014, ApJ, 785, 151
Howarth, I. D. 1983, MNRAS, 203, 301
Hunter, I., Dufton, P. L., Ryans, R. S. I., et al. 2005, A&A, 436, 687
Hunter, I., Dufton, P. L., Smartt, S. J., et al. 2007, A&A, 466, 277
Hunter, I., Brott, I., Lennon, D. J., et al. 2008a, ApJ, 676, L29
Hunter, I., Lennon, D. J., Dufton, P. L., et al. 2008b, A&A, 479, 541
Hunter, I., Brott, I., Langer, N., et al. 2009, A&A, 496, 841
Hutchings, J. B., Crampton, D., & Cowley, A. P. 1978, ApJ, 225, 548
Isserstedt, J. 1975, A&AS, 19, 259
Isserstedt, J. 1979, A&AS, 38, 239
Isserstedt, J. 1982, A&AS, 50, 7
James, B. L., Berg, D. A., King, T., et al. 2022, ApJS, 262, 37
Kaper, L., Henrichs, H. F., Nichols, J. S., et al. 1996, A&AS, 116, 257
Kaper, L., Henrichs, H. F., Nichols, J. S., & Telting, J. H. 1999, A&A, 344, 231
Kausch, W., Noll, S., Smette, A., et al. 2015, A&A, 576, A78
Kehrig, C., Vílchez, J. M., Pérez-Montero, E., et al. 2015, ApJ, 801, L28
Koenigsberger, G., Morrell, N., Hillier, D. J., et al. 2014, AJ, 148, 62
Köhler, K., Langer, N., de Koter, A., et al. 2015, A&A, 573, A71
Korn, A. J., Becker, S. R., Gummersbach, C. A., & Wolf, B. 2000, A&A, 353, 655
Korn, A. J., Nieva, M. F., Daflon, S., & Cunha, K. 2005, ApJ, 633, 899
Kurt, C. M., & Dufour, R. J. 1998, Rev. Mex. Astron. Astrofis. Conf. Ser., 7, 202
Krtička, J., & Kubát, J. 2017, A&A, 606, A31
Krtička, J., & Kubát, J. 2018, A&A, 612, A20
Kruckow, M. U., Tauris, T. M., Langer, N., et al. 2016, A&A, 596, A58
Kudritzki, R. P. 2002, ApJ, 577, 389
Lamb, J. B., Oey, M. S., Graus, A. S., Adams, F. C., & Segura-Cox, D. M. 2013, ApJ, 763, 101
Lamb, J. B., Oey, M. S., Segura-Cox, D. M., et al. 2016, ApJ, 817, 113
Lamers, H. J. G. L. M., Cerruti-Sola, M., & Perinotto, M. 1987, ApJ, 314, 726
Lamers, H. J. G. L. M., Zickgraf, F.-J., de Winter, D., Houziaux, L., & Zorec, J. 1998, A&A, 340, 117
Lanz, T., & Hubeny, I. 2003, ApJS, 146, 417
Laplace, E., Götberg, Y., de Mink, S. E., Justham, S., & Farmer, R. 2020, A&A, 637, A6
Lebouteiller, V., Bernard-Salas, J., Brandl, B., et al. 2008, ApJ, 680, 398
Lecoanet, D., Bowman, D. M., & Van Reeth, T. 2022, MNRAS, 512, L16
Lennon, D. J. 1997, A&A, 317, 871
Lorenzo, M., Garcia, M., Najarro, F., et al. 2022, MNRAS, 516, 4164
Maeder, A. 1987, A&A, 178, 159
Maeder, A., Przybilla, N., Nieva, M.-F., et al. 2014, A&A, 565, A39
Magg, E., Bergemann, M., Serenelli, A., et al. 2022, A&A, 661, A140
Mahy, L., Sana, H., Abdul-Masih, M., et al. 2020, A&A, 634, A118
Maíz Apellániz, J., Evans, C. J., Barbá, R. H., et al. 2014, A&A, 564, A63
Maíz Apellániz, J., Barbá, R. H., Caballero, J. A., Bohlin, R. C., & Fariña, C. 2021, MNRAS, 501, 2487
Mandel, I., & de Mink, S. E. 2016, MNRAS, 458, 2634
Marcolino, W. L. F., Bouret, J. C., Rocha-Pinto, H. J., Bernini-Peron, M., & Vink, J. S. 2022, MNRAS, 511, 5104
Martins, F., & Plez, B. 2006, A&A, 457, 637
Martins, F., Hillier, D. J., Bouret, J. C., et al. 2009, A&A, 495, 257
Massa, D., Fullerton, A. W., Nichols, J. S., et al. 1995, ApJ, 452, L53
Massa, D., Fullerton, A. W., Sonneborn, G., & Hutchings, J. B. 2003, ApJ, 586, 996
Massey, P. 2002, ApJS, 141, 81
Massey, P., Parker, J. W., & Garmany, C. D. 1989, AJ, 98, 1305
Massey, P., Lang, C. C., Degioia-Eastwood, K., & Garmany, C. D. 1995, ApJ, 438, 188
Massey, P., Waterhouse, E., & DeGioia-Eastwood, K. 2000, AJ, 119, 2214
Massey, P., Bresolin, F., Kudritzki, R. P., Puls, J., & Pauldrach, A. W. A. 2004, ApJ, 608, 1001
Massey, P., Puls, J., Pauldrach, A. W. A., et al. 2005, ApJ, 627, 477
Massey, P., Olsen, K. A. G., Hodge, P. W., et al. 2007, AJ, 133, 2393
Massey, P., Zangari, A. M., Morrell, N. I., et al. 2009, ApJ, 692, 618
Massey, P., Neugent, K. F., & Morrell, N. 2017, ApJ, 837, 122
Mathews, W. G. 1967, ApJ, 147, 965
McEvoy, C. M., Dufton, P. L., Evans, C. J., et al. 2015, A&A, 575, A70
Mennickent, R. E., Cidale, L., Pietrzyński, G., Gieren, W., & Sabogal, B. 2006, A&A, 457, 949
Moehler, S., Modigliani, A., Freudling, W., et al. 2014, A&A, 568, A9
Mokiem, M. R., de Koter, A., Evans, C. J., et al. 2006, A&A, 456, 1131
Mokiem, M. R., de Koter, A., Evans, C. J., et al. 2007a, A&A, 465, 1003
Mokiem, M. R., de Koter, A., Vink, J. S., et al. 2007b, A&A, 473, 603
Morel, T., Castro, N., Fossati, L., et al. 2015, in New Windows on Massive Stars, eds. G. Meynet, C. Georgy, J. Groh, & P. Stee, 307, 342
Morrell, N. I., Niemela, V. S., Barbá, R. H., et al. 1999, in Revista Mexicana de Astronomia y Astrofisica Conference Series, eds. N. I. Morrell, V. S. Niemela, & R. H. Barbá, Rev. Mex. Astron. Astrofis. Conf. Ser., 8, 149
Negueruela, I., & Coe, M. J. 2002, A&A, 385, 517
Niemela, V., & Gamen, R. 2004, New A Rev., 48, 727
Niemela, V. S. 2002, in Extragalactic Star Clusters, eds. D. P. Geisler, E. K. Grebel, & D. Minniti, 207, 202
Oey, M. S. 1996, ApJ, 467, 666
Oey, M. S., & Kennicutt, R. C. 1997, MNRAS, 291, 827
Oey, M. S., & Smedley, S. A. 1998, AJ, 116, 1263
Oskinova, L. M., Hamann, W. R., & Feldmeier, A. 2007, A&A, 476, 1331
Ostrov, P. G., & Lapasset, E. 2003, MNRAS, 338, 141
Palmerio, J. T., Vergani, S. D., Salvaterra, R., et al. 2019, A&A, 623, A26
Parker, J. W. 1993, AJ, 106, 560
Parker, J. W., Garmany, C. D., Massey, P., & Walborn, N. R. 1992, AJ, 103, 1205
Pauli, D., Oskinova, L. M., Hamann, W. R., et al. 2022, A&A, 659, A9
Pawlak, M., Graczyk, D., Soszyński, I., et al. 2013, Acta Astron., 63, 323
Paxton, B., Bildsten, L., Dotter, A., et al. 2011, ApJS, 192, 3
Paxton, B., Cantiello, M., Arras, P., et al. 2013, ApJS, 208, 4
Paxton, B., Marchant, P., Schwab, J., et al. 2015, ApJS, 220, 15
Paxton, B., Schwab, J., Bauer, E. B., et al. 2018, ApJS, 234, 34
Paxton, B., Smolec, R., Schwab, J., et al. 2019, ApJS, 243, 10
Peimbert, A. 2003, ApJ, 584, 735
Pellegrini, E. W., Oey, M. S., Winkler, P. F., et al. 2012, ApJ, 755, 40
Penny, L. R., & Gies, D. R. 2009, ApJ, 700, 844
Penny, L. R., Sprague, A. J., Seago, G., & Gies, D. R. 2004, ApJ, 617, 1316
Petrov, B., Vink, J. S., & Gräfener, G. 2016, MNRAS, 458, 1999
Pietrzyński, G., Graczyk, D., Gallenne, A., et al. 2019, Nature, 567, 200
Prevot, M. L., Lequeux, J., Maurice, E., Prevot, L., & Rocca-Volmerange, B. 1984, A&A, 132, 389
Prinja, R. K., & Crowther, P. A. 1998, MNRAS, 300, 828
Prinja, R. K., Barlow, M. J., & Howarth, I. D. 1990, ApJ, 361, 607
Przybilla, N., Firnstein, M., Nieva, M. F., Meynet, G., & Maeder, A. 2010, A&A, 517, A38
Puls, J., Kudritzki, R. P., Herrero, A., et al. 1996, A&A, 305, 171
Puls, J., Springmann, U., & Lennon, M. 2000, A&AS, 141, 23
Puls, J., Urbaneja, M. A., Venero, R., et al. 2005, A&A, 435, 669
Puls, J., Vink, J. S., & Najarro, F. 2008, A&A Rv, 16, 209
Puls, J., Najarro, F., Sundqvist, J. O., & Sen, K. 2020, A&A, 642, A172
Quimby, R. M., Kulkarni, S. R., Kasliwal, M. M., et al. 2011, Nature, 474, 487
Ramírez-Agudelo, O. H., Sana, H., de Koter, A., et al. 2017, A&A, 600, A81
Ramachandran, V., Hainich, R., Hamann, W. R., et al. 2018a, A&A, 609, A7
Ramachandran, V., Hamann, W. R., Hainich, R., et al. 2018b, A&A, 615, A40
Ramachandran, V., Hamann, W. R., Oskinova, L. M., et al. 2019, A&A, 625, A104
Ramírez-Agudelo, O. H., Simón-Díaz, S., Sana, H., et al. 2013, A&A, 560, A29
Reynolds, A. P., Hilditch, R. W., Bell, S. A., & Hill, G. 1993, MNRAS, 261, 337
Rickard, M. J., Hainich, R., Hamann, W. R., et al. 2022, A&A, 666, A189
Ricker, G. R., Winn, J. N., Vanderspek, R., et al. 2015, J. Astron. Telescopes Instrum. Syst., 1, 014003
Ritchie, B. W., Stroud, V. E., Evans, C. J., et al. 2012, A&A, 537, A29
Rivero González, J. G., Puls, J., Massey, P., & Najarro, F. 2012a, A&A, 543, A95
Rivero González, J. G., Puls, J., Najarro, F., & Brott, I. 2012b, A&A, 537, A79
Rolleston, W. R. J., Venn, K., Tolstoy, E., & Dufton, P. L. 2003, A&A, 400, 21
Roman-Duval, J., Proffitt, C. R., Taylor, J. M., et al. 2020, Res. Notes Am. Astron. Soc., 4, 205
Rousseau, J., Martin, N., Prévot, L., et al. 1978, A&AS, 31, 243
Sabín-Sanjulián, C., Simón-Díaz, S., Herrero, A., et al. 2014, A&A, 564, A39
Sabín-Sanjulián, C., Simón-Díaz, S., Herrero, A., et al. 2017, A&A, 601, A79
Salmon, S., Montalbán, J., Morel, T., et al. 2012, MNRAS, 422, 3460
Salmon, S. J. A. J., Eggenberger, P., Montalbán, J., et al. 2022, A&A, 659, A142
Sana, H., de Mink, S. E., de Koter, A., et al. 2012, Science, 337, 444
Sana, H., de Koter, A., de Mink, S. E., et al. 2013, A&A, 550, A107
Sander, A. A. C., & Vink, J. S. 2020, MNRAS, 499, 873
Sander, A., Shenar, T., Hainich, R., et al. 2015, A&A, 577, A13
Sander, A. A. C., Hamann, W. R., Todt, H., Hainich, R., & Shenar, T. 2017, A&A, 603, A86
Sander, A. A. C., Vink, J. S., & Hamann, W. R. 2020, MNRAS, 491, 4406
Sanduleak, N. 1969, AJ, 74, 877
Santolaya-Rey, A. E., Puls, J., & Herrero, A. 1997, A&A, 323, 488
Schmidt-Kaler, T., Gochermann, J., Oestreicher, M. O., et al. 1999, MNRAS, 306, 279
Schneider, F. R. N., Langer, N., de Koter, A., et al. 2014, A&A, 570, A66
Schnurr, O., Moffat, A. F. J., St-Louis, N., Morrell, N. I., & Guerrero, M. A. 2008, MNRAS, 389, 806

Seaton, M. J. 1979, MNRAS, 187, 73
Selman, F., Melnick, J., Bosch, G., & Terlevich, R. 1999, A&A, 341, 98
Shenar, T., Hainich, R., Todt, H., et al. 2016, A&A, 591, A22
Shenar, T., Hainich, R., Todt, H., et al. 2018, A&A, 616, A103
Shenar, T., Sablowski, D. P., Hainich, R., et al. 2019, A&A, 627, A151
Shenar, T., Sana, H., Mahy, L., et al. 2022, A&A, 665, A148
Shirazi, M., & Brinchmann, J. 2012, MNRAS, 421, 1043
Simón-Díaz, S. 2020, Reviews in Frontiers of Modern Astrophysics (FromSpace Debris to Cosmology: From Space Debris to Cosmology), 155
Simón-Díaz, S., & Herrero, A. 2014, A&A, 562, A135
Sirressi, M., Adamo, A., Hayes, M., et al. 2022, AJ, 164, 208
Smette, A., Sana, H., Noll, S., et al. 2015, A&A, 576, A77
Smith, L. F., Shara, M. M., & Moffat, A. F. J. 1990, ApJ, 348, 471
Smith, L. F., Shara, M. M., & Moffat, A. F. J. 1996, MNRAS, 281, 163
Smith Neubig, M. M., & Bruhweiler, F. C. 1997, AJ, 114, 1951
Spitzer, L. 1978, Physical Processes in the Interstellar Medium (New York: Wiley- Interscience)
Steidel, C. C., Strom, A. L., Pettini, M., et al. 2016, ApJ, 826, 159
Strom, A. L., Rudie, G. C., Steidel, C. C., & Trainor, R. F. 2022, ApJ, 925, 116
Sundqvist, J. O., Owocki, S. P., & Puls, J. 2018, A&A, 611, A17
Sundqvist, J. O., Björklund, R., Puls, J., & Najarro, F. 2019, A&A, 632, A126
Tautvaišienė, G., Geisler, D., Wallerstein, G., et al. 2007, AJ, 134, 2318
Tchernyshyov, K., Meixner, M., Seale, J., et al. 2015, ApJ, 811, 78
Testor, G., & Niemela, V. 1998, A&AS, 130, 527
Toribio San Cipriano, L., Domínguez-Guzmán, G., Esteban, C., et al. 2017, MNRAS, 467, 3759
Tramper, F., Sana, H., de Koter, A., Kaper, L., & Ramírez-Agudelo, O. H. 2014, A&A, 572, A36
Trundle, C., & Lennon, D. J. 2005, A&A, 434, 677
Trundle, C., Lennon, D. J., Puls, J., & Dufton, P. L. 2004, A&A, 417, 217
Trundle, C., Dufton, P. L., Hunter, I., et al. 2007, A&A, 471, 625
Tsamis, Y. G., Barlow, M. J., Liu, X. W., Danziger, I. J., & Storey, P. J. 2003, MNRAS, 338, 687
ud-Doula, A., Owocki, S. P., Townsend, R. H. D., et al. 2008, MNRAS, 385, 97
Ulaczyk, K., Szymański, M. K., Udalski, A., et al. 2013, Acta Astron., 63, 159
Urbaneja, M. A., Kudritzki, R. P., Gieren, W., et al. 2017, AJ, 154, 102
van Loon, J. T., Bailey, M., Tatton, B. L., et al. 2013, A&A, 550, A108
Venn, K. A. 1999, ApJ, 518, 405
Vernet, J., Dekker, H., D'Odorico, S., et al. 2011, A&A, 536, A105
Verro, K., Trager, S. C., Peletier, R. F., et al. 2022, A&A, 660, A34
Vink, J. S., de Koter, A., & Lamers, H. J. G. L. M. 1999, A&A, 350, 181
Vink, J. S., de Koter, A., & Lamers, H. J. G. L. M. 2000, A&A, 362, 295
Vink, J. S., de Koter, A., & Lamers, H. J. G. L. M. 2001, A&A, 369, 574
Voges, E. S., Oey, M. S., Walterbos, R. A. M., & Wilkinson, T. M. 2008, AJ, 135, 1291
Vreeswijk, P. M., Ellison, S. L., Ledoux, C., et al. 2004, A&A, 419, 927
Wade, G. A., Neiner, C., Alecian, E., et al. 2016, MNRAS, 456, 2
Walborn, N. R. 1977, ApJ, 215, 53
Walborn, N. R. 1983, ApJ, 265, 716
Walborn, N. R., Lennon, D. J., Haser, S. M., Kudritzki, R.-P., & Voels, S. A. 1995, PASP, 107, 104
Walborn, N. R., Lennon, D. J., Heap, S. R., et al. 2000, PASP, 112, 1243
Walborn, N. R., Fullerton, A. W., Crowther, P. A., et al. 2002a, ApJS, 141, 443
Walborn, N. R., Howarth, I. D., Lennon, D. J., et al. 2002b, AJ, 123, 2754
Walborn, N. R., Morrell, N. I., Howarth, I. D., et al. 2004, ApJ, 608, 1028
Walborn, N. R., Howarth, I. D., Evans, C. J., et al. 2010, AJ, 139, 1283
Walborn, N. R., Sana, H., Simón-Díaz, S., et al. 2014, A&A, 564, A40
Weaver, R., McCray, R., Castor, J., Shapiro, P., & Moore, R. 1977, ApJ, 218, 377
Welty, D. E., Federman, S. R., Gredel, R., Thorburn, J. A., & Lambert, D. L. 2006, ApJS, 165, 138
Yoon, S. C., & Langer, N. 2005, A&A, 443, 643
Yoon, S.-C., Dessart, L., & Clocchiatti, A. 2017, ApJ, 840, 10
Zastrow, J., Oey, M. S., & Pellegrini, E. W. 2013, ApJ, 769, 94
Zaritsky, D., Harris, J., Thompson, I. B., Grebel, E. K., & Massey, P. 2002, AJ, 123, 855
Zaritsky, D., Harris, J., Thompson, I. B., & Grebel, E. K. 2004, AJ, 128, 1606
Zasche, P., Wolf, M., & Vraštil, J. 2017, MNRAS, 472, 2241
Zickgraf, F. J., Kovacs, J., Wolf, B., et al. 1996, A&A, 309, 505

[1] Armagh Observatory and Planetarium, College Hill, BT61 9DG Armagh, UK
e-mail: jorick.vink@armagh.ac.uk
[2] ESO – European Organisation for Astronomical Research in the Southern Hemisphere, Alonso de Cordova 3107, Vitacura, Santiago de Chile, Chile
e-mail: amehner@eso.org
[3] Dept of Physics & Astronomy, University of Sheffield, Hounsfield Road, Sheffield S3 7RH, UK
e-mail: paul.crowther@sheffield.ac.uk
[4] Institute of Astronomy, KU Leuven, Celestijnenlaan 200D, 3001 Leuven, Belgium
[5] Penn State Scranton, 120 Ridge View Drive, Dunmore, PA 18512, USA
[6] Centre for Extragalactic Astronomy, Department of Physics, Durham University, South Road, Durham DH1 3LE, UK
[7] Institute for Computational Cosmology, Department of Physics, University of Durham, South Road, Durham DH1 3LE, UK
[8] Department of Physics and Astronomy, East Tennessee State University, Johnson City, TN 37614, USA
[9] Department of Physics and Astronomy & Pittsburgh Particle Physics, Astrophysics and Cosmology Center (PITT PACC), University of Pittsburgh, 3941 O'Hara Street, Pittsburgh, PA 15260, USA
[10] Astronomický ústav, Akademie věd České republiky, 251 65 Ondřejov, Czech Republic
[11] Instituto de Astrofisica de Canarias, 38200 La Laguna, Tenerife, Spain
[12] Dpto. Astrofisica, Universidad de La Laguna, 38 205 La Laguna, Tenerife, Spain
[13] Argelander Institute für Astronomie der Universität Bonn, Auf dem Hügel 71, 53121 Bonn, Germany
[14] LUPM, Université de Montpellier, CNRS, Place Eugène Bataillon, 34095 Montpellier, France
[15] ESO – European Organisation for Astronomical Research in the Southern Hemisphere, Karl-Schwarzschild-Str. 2, 85748 Garching b. München, Germany
[16] Las Campanas Observatory, Carnegie Observatories, Casilla 601, La Serena, Chile
[17] Anton Pannekoek Institute for Astronomy, Universiteit van Amsterdam, Science Park 904, 1098 XH Amsterdam, The Netherlands
[18] Leiden Observatory, Leiden University, 2300 RA Leiden, The Netherlands
[19] Center for Computational Astrophysics, Division of Science, National Astronomical Observatory of Japan, 2-21-1, Osawa, Mitaka, Tokyo 181-8588, Japan
[20] Zentrum für Astronomie der Universität Heidelberg, Rechen-Institut, Mönchhofstr. 12-14, 69120 Heidelberg, Germany
[21] NAT – Universidade Cidade de Sao Paulo, Rua Galvao Bueno, 868, São Paulo, Brazil
[22] Department of Physics and Astronomy, University College London, Gower Street, London WC1E 6BT, UK
[23] Fakultät für Physik, Universität Duisburg-Essen, Lotharstraße 1, 47057 Duisburg, Germany
[24] Gemini Observatory/NSF's NOIRLab, Casilla 603, La Serena, Chile
[25] University of Michigan, Department of Astronomy, 323 West Hall, Ann Arbor, MI 48109, USA
[26] Institute for Physics and Astronomy, University Potsdam, 14476 Potsdam, Germany
[27] Kavli Institute for Theoretical Physics, Kohn Hall, University of California, Santa Barbara, CA 93106, USA
[28] European Space Agency (ESA), ESA Office, Space Telescope Science Institute, 3700 San Martin Drive, Baltimore, MD 21218, USA
[29] Centro de Astrobiología (CAB), CSIC-INTA, Campus ESAC. C. bajo del castillo s/n, 28 692 Madrid, Spain
[30] Heidelberger Institut für Theoretische Studien, Schloss-Wolfsbrunnenweg 35, 69118 Heidelberg, Germany
[31] Center for Astrophysics and Space Astronomy, University of Colorado Boulder, Boulder, CO 80309-0389, USA
[32] Aix Marseille Univ, CNRS, CNES, LAM, Marseille, France
[33] Département de physique, Université de Montréal, Campus MIL, 1375 Thérèse-Lavoie-Roux, Montréal, (QC) H2V 0B3, Canada
[34] Royal Observatory of Belgium, Avenue circulaire/Ringlaan 3, 1180 Brussels, Belgium

[35] Rutgers University, Department of Physics and Astronomy, 136 Frelinghuysen Road, Piscataway, NJ 08854, USA
[36] Lennard-Jones Laboratories, Keele University, Keele ST5 5BG, UK
[37] The Observatories of the Carnegie Institution for Science, 813 Santa Barbara Street, CA 91101 Pasadena, USA
[38] Centro de Astrobiología (CAB), CSIC-INTA, Ctra. Torrejón a Ajalvir km 4., 28850 Torrejón de Ardoz, Madrid, Spain
[39] Departamento de Física Aplicada, Universidad de Alicante, 03 690, San Vicente del Raspeig, Alicante, Spain
[40] Department of Physics and Astronomy, Howard University, Washington, DC 20059, USA
[41] Observatório do Valongo, Universidade Federal do Rio de Janeiro, Ladeira Pedro Antônio 43, Rio de Janeiro, CEP 20080-090, Brazil
[42] Instituto de Astrofísica de Andalucía – CSIC, Glorieta de la Astronomía s/n, 18008 Granada, Spain
[43] Center for Research and Exploration in Space Science and Technology, and X-ray Astrophysics Laboratory, NASA/GSFC, Greenbelt, MD 20771, USA
[44] Space Telescope Science Institute, 3700 San Martin Dr, Baltimore, MD 21218, USA
[45] Max Planck Institut für Astronomie, Königstuhl 17, 69117 Heidelberg, Germany
[46] Max Planck Institut für Astrophysik, Karl-Schwarzschild-Strasse 1, 85741 Garching, Germany
[47] Centro Universitário FEI, Dept. de Física. Av. Humberto Alencar de Castelo Branco, 3972, São Bernardo do Campo, SP, CEP 09850-901, Brazil
[48] IAASARS, National Observatory of Athens, 15236 Penteli, Greece
[49] Department of Astrophysics/IMAPP, Radboud University Nijmegen, PO Box 9010, 6500 GL Nijmegen, The Netherlands
[50] Instituto de Astronomía, Universidad Nacional Autónoma de México, Unidad Académica en Ensenada, Km 103 Carr. Tijuana-Ensenada, Ensenada, B.C. CP 22860, Mexico
[51] National Solar Observatory, 22 Ohi'a Ku St, Makawao, HI 96768, USA
[52] Institute of Astrophysics, FORTH, 71110 Heraklion, Greece
[53] Yunnan Observatories, Chinese Academy of Sciences, Kunming 650216 Yunnan, PR China

Appendix A: The XShootU collaboration

A.1. Organisation (WG 1)

XShootU is a project with a wide-scale community approach. The collaboration is organised into 14 WGs that anyone can join: (1) Organisation, (2) Data Reduction and Calibration, (3) Stellar Atmospheres and Benchmarking, (4) Wind Structure, (5) Stellar Evolution Modelling, (6) Stellar Libraries, (7) Population Synthesis, (8) Interstellar Medium, (9) Massive Star Feedback, (10) Stripped Stars, (11), Auxiliary/New Data, (12) Pulsations, (13) Magnetic Fields, and (14) Unusual Objects.

A.2. Data Reduction and Calibration (WG 2)

The detailed description of the UVB and VIS higher level data products will be associated with DR1 (Sana et al., in prep., XShootU II). The data reduction of the NIR spectra will become part of DR2.

A.3. Stellar Atmospheres and Benchmarking (WG 3)

WG 3 was set up to foster discussions and cooperation between researchers performing the spectroscopic analysis of the XShootU datasets. Part of this work is described in the main part of the paper. Several sub-groups were organised by WG 3 members to address specific science questions and topics of interest. This ranges from the determination of the full photospheric and wind properties of the sample at large, to very specific issues such as studying the effects of rotational mixing on stars with different masses/ages through abundance studies. The three main codes that are employed for the spectroscopic analysis are the NLTE expanding wind codes CMFGEN, FASTWIND, and PoWR (Hillier & Miller 1998; Puls et al. 2020; Gräfener et al. 2002), and the plane parallel NLTE code TLUSTY for stars without strong winds.

A.4. Wind Structure (WG 4)

Winds of massive, hot stars are time-dependent and highly structured on small and large spatial scales (see the overviews in Puls et al. 2008; Hamann et al. 2008). It has been shown that properties of structured winds have an enormous impact on empirical estimates of mass-loss rates, and thus on our understanding of stellar evolution. However, the question to which extent $\dot{M}$ is influenced by wind structures remains. WG 4 studies the clumping dependence on spectral and luminosity classes at different Z. Spectral modelling is performed using state-of-the-art model atmosphere codes (see WG 3), which can treat clumping properties with different levels of sophistication. Wind clumping is usually treated in the 'micro-clumping' (i.e. optically thin clumps at all frequencies) or 'macro-clumping' (i.e. arbitrary optical thickness of clumps) approximations, still assuming a void inter-clump medium and a smooth velocity field (e.g. CMFGEN, PoWR, and METUJE; Krtička & Kubát 2017, 2018).

A.5. Stellar Evolution Modelling (WG 5)

The objectives of the stellar evolution group fall into two categories. The first one is to provide up to date sets of stellar evolution models covering not only the parameter space of initial conditions but also that of uncertain physical prescriptions such as overshooting. Following the work of Schneider et al. (2014), we also provide open source tools[7] for performing Bayesian inference of observed systems and inferring their initial properties given a set of simulations. Even though the XShootU sample was designed to exclude known binary stars, it is possible that such a sample contains large numbers of binary products. Therefore, extended grids of binary evolution will also be constructed and incorporated into the Bayesian inference framework under construction. Our simulations will be coded using the MESA software instrument (Paxton et al. 2011, 2013, 2015, 2018, 2019), but our Bayesian tools are designed to easily incorporate simulations from other stellar evolution simulations, allowing us to establish systematic biases on our theoretical models. The second objective of the WG will be the development of tailored evolutionary models for specific objects of interest found within the XShootU sample.

A.6. Stellar Libraries (WG 6)

Stellar spectral libraries are one of the main ingredients of stellar population synthesis models, which in turn are powerful tools in the study of fundamental properties of unresolved stellar systems. One of the major deficiencies of the empirical libraries available today is the coverage of hot and young stars at low Z (Hill et al. 2022). A variety of empirical stellar spectral libraries, collected with different primary goals, are publicly available (see Table 1 in Verro et al. 2021 for a recent summary). In terms of spectral resolving power, only the X-shooter Spectral Library (XSL) and ELODIE are comparable to the XShootU dataset. ULLYSES + XShootU is by far the most complete, highest-S/N, and highest resolution library of hot, massive stars with the broadest spectral coverage. While numerous libraries for low-mass stars are available, these libraries are incomplete at high masses. To illustrate this point, we compared the ULLYSES + XShootU target sample with the XSL library (Verro et al. 2022), which was designed for stellar population synthesis. In Fig. A.1 we show the HR diagram coverage of the XSL library, which shows the lack of massive OB stars at any Z. ULLYSES + XShootU perfectly complement the missing parameter space of the XSL library. In combination, the two libraries allow self-consistent population synthesis models (see WG 7) of systems hosting both young and old stars.

A.7. Population Synthesis (WG 7)

Population synthesis models are called semi-empirical if the stellar evolution tracks are theoretical but the individual stellar spectra are observed, and fully theoretical when both are calculated. XShootU observations will enable improvements of semi-empirical models because they will provide the most complete spectral library to date. In addition, the XShootU observations will guide new generations of atmosphere and evolution models, which will help improve fully theoretical population synthesis models. The new empirical library of LMC + SMC UV-to-NIR massive-star spectra built by the ULLYSES and XShootU projects will replace the Starburst99 LMC + SMC library, greatly improving the realism of population synthesis predictions. Once the library is implemented in Starburst99, corresponding Cloudy (Ferland et al. 2017) photoionisation models will be computed in order to account for the contribution of the ionised gas and dust to the integrated light of young OB star populations. The models, which will be publicly available,

[7] An early version of these tools can be found at https://github.com/orlox/StarStats.jl

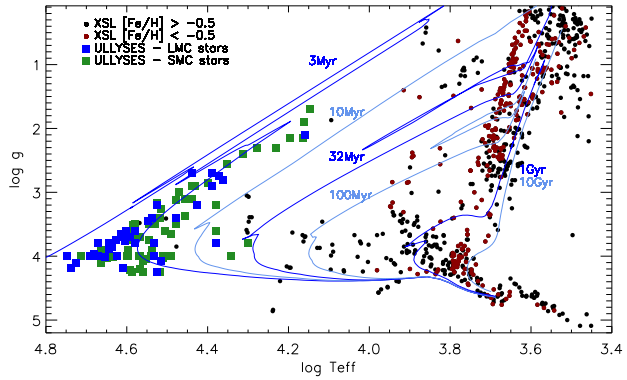

Fig. A.1. Comparison of the ULLYSES (blue: LMC; green: SMC) and XSL libraries. XSL stars (filled circles) are separated by metallicity: [Fe/H] > −0.5 (black) and [Fe/H] < −0.5 (dark red). Temperatures, gravities, and metallicities of the ULLYSES stars in this figure were obtained from the literature. Solid lines are Geneva isochrones for $Z_\odot$ and various ages (Ekström et al. 2012).

will be used to interpret existing and future observations of star-forming and starburst galaxies with similar metallicities, in particular those from CLASSY (Berg et al. 2022; James et al. 2022) high-resolution ($R \sim 15\,000$) Far-UV spectral database of 45 nearby ($0.002 < z < 0.182$) star-forming galaxies, the majority of which have LMC- or SMC-like metallicities.

A.8. Interstellar Medium (WG 8)

The intervening ISM along the line of sight to each target star will impact the observed UV and optical spectra. Cool atomic and molecular gas produces absorption features superimposed on stellar photospheric and wind lines. Furthermore, dust in the Milky Way and the host galaxy extinguishes and reddens the stellar spectra. These effects must be accounted for to reliably analyse stellar features, but also enable ISM science that is interesting in its own right. Due to the nature of the UV-based selection process of the target sample and the fact that most OB stars in the Magellanic Clouds experience low extinctions ($E(B-V) < 0.20$ mag), strong ISM signatures are not expected in the optical and NIR X-shooter spectra. Nevertheless, clear signatures are expected in strong atomic lines such as the Na I $\lambda\lambda$5889.951,5895.924 and Ca II $\lambda\lambda$3933.663,3968.468 doublets. For the targets with the strongest extinctions, detection are expected for some molecular lines, such as CH λ4300.313 and CH+ λ4232.548, and strong diffuse interstellar bands, such as those at 4428 Å, 5780.5 Å, 5797.1 Å, and 6614 Å. These lines have been well studied for Galactic targets but less so for objects in the Magellanic Clouds (though see e.g. Ehrenfreund et al. 2002; Welty et al. 2006; Cox et al. 2006, 2007; van Loon et al. 2013; Bailey et al. 2015). The coverage of the significantly less studied wavelength region between 3200 − 3800 Å could provide detections of some lines such as Ti I λ3729.8069 and Ti II λ3383.759. In addition, the flux calibration of the X-shooter spectra will provide insights into the Magellanic Cloud extinction laws (Maíz Apellániz et al. 2014) and possibly detect the recently discovered very broad absorption band centred on 7700 Å (Maíz Apellániz et al. 2021).

A.9. Massive Star Formation and Feedback (WG 9)

The energy output from young OB stars creates expanding H II regions that are over-pressurised with respect to their surroundings by photoionisation, radiation pressure on dust grains, and shock heating by stellar winds (Mathews 1967; Weaver et al. 1977; Spitzer 1978). Key stellar properties for the structure and dynamics of these regions are the flux in far-UV and extreme-UV photons and the stellar wind mass-loss rate and terminal velocity. The density distribution, chemistry, and equilibrium temperature of the photoionised gas also play important roles (Ferland et al. 2017). Because the LMC and SMC have substantially lower metallicities than the Galaxy, their H II regions are ideal test cases for the impacts of stellar ionising flux (Voges et al. 2008; Oey & Kennicutt 1997) and winds (e.g. Oey 1996; Oey & Smedley 1998) in low-metallicity environments typical of high-redshift galaxies. The XShootU dataset in the Magellanic Clouds represents a significant opportunity to advance the state of the art in our understanding of how stars shape their environment. WG9 has identified a sample of relatively isolated XShootU stars that reside inside H II regions identified in the MCELS survey (Pellegrini et al. 2012). These single-star H II regions are valuable tools for calibrating stellar atmosphere models (like those produced by WG 3) by comparing observed nebular emission lines to photoionisation models adopting those model atmospheres as the ionising sources (Zastrow et al. 2013). Combining stellar properties inferred from the XShootU spectra with the observed structure and emission of the ionised gas in these regions will clarify the role stars play in shaping their environment.

A.10. Stripped Stars (WG 10)

Stars stripped of their hydrogen-rich envelopes via mass transfer or common envelope ejection in binary systems are thought to be the fate of a third of all massive stars (Sana et al. 2012). In fact, in a continuously star-forming population, a few percent of all massive stars should be accompanied by a stripped companion. Binary-stripped stars are the exposed helium cores of their progenitors. During the long-lived phase of core helium burning these stars are small ($R_\star \lesssim 1\ R_\odot$), hot ($T_{\rm eff} \sim 50-100$ kK), compact ($\log g \sim 5$), helium-rich ($Y_{\rm surf} \sim 0.5-1$), and hydrogen-poor ($X_{\rm surf} \sim 0-0.5$), but span a range of luminosities ($1-10^6\ L_\odot$) and masses ($\sim 0.5-10\ M_\odot$) (Götberg et al. 2018). After core-helium exhaustion, they can expand to giant sizes, depending on the fraction of hydrogen they retain, and appear as helium-enriched blue, yellow, or red supergiants (Yoon et al. 2017; Laplace et al. 2020). ULLYSES offers an excellent sample to search for hot binary-stripped stars that are sufficiently massive to explode as SNe. Especially with the effort to exclude apparent binaries from the target sample, the likelihood of having a few hidden binary-stripped companions increases, as they are not expected to significantly contribute to the optical flux or to cause large radial velocities. While UV spectra will be crucial for this analysis, the optical spectra are needed for stellar characterisation of both the binary-stripped star and the accretor star. We expect that discovering binary-stripped star + OB star systems in the ULLYSES sample will help constrain uncertainties, such as how common and efficient mass transfer is, and exactly how the two stars are affected by such mass transfer.

A.11. Auxiliary/New Data (WG 11)

There are multiple ways in which auxiliary data can help increase the value of the ULLYSES/XShootU library, including different wavelength regimes (e.g. X-rays) and observing strategies. For example, the intermediate spectral resolving power of the X-shooter data only partially resolves spectral lines, especially for stars with low projected rotational velocities ($v \sin i$),

and higher resolution spectra are needed for a detailed spectroscopic analysis. WG 11 will provide high-resolution optical spectroscopy of a selection of slow rotating ULLYSES targets. Targets were selected on the basis of showing narrow, resolved C III 1176 Å lines in their UV spectra or having low $v \sin i$ reported in the literature. Between December 2021 and December 2022, we obtained high resolution ($R \sim 40\,000$) and high S/N (~ 200 in the 4100 Å region) optical spectra with the 6.5m Magellan Clay telescope (+MIKE spectrograph) for 48 ULLYSES targets. Basic reductions confirmed the high quality of the data, and final reductions are underway. The Magellan/MIKE data will be made available to the massive stars community. WG11 also plans to organise archival searches aimed to identify data that will enhance the ULLYSES/XShootU library:

– High spectral resolution optical spectra of ULLYSES targets, for example obtained with the UVES, FLAMES, FEROS, and HARPS instruments.
– UV spectra obtained with IUE, FUSE, and HST.

A.12. Pulsations (WG 12)

The study of spectroscopic variability in XShootU targets is naturally supported by the analysis of time-series photometry from the NASA Transiting Exoplanet Survey Satellite (TESS) mission (Ricker et al. 2015). The LMC is within the southern continuous viewing zone of the TESS mission, such that all XShootU stars in the LMC have continuous light curves spanning 1 yr. TESS light curves have been used to demonstrate that heat-driven pulsations and the signatures of rotational modulation are common in early-type main-sequence stars in the Galaxy (David-Uraz et al. 2019; Burssens et al. 2020). Whereas, the brightest massive stars in the Magellanic Clouds (i.e. OB supergiants) have light curves dominated by stochastic low-frequency variability (Bowman et al. 2019). Interestingly, in low-metallicity environments such as the Magellanic Clouds, the driving of heat-driven pulsations is less efficient (Salmon et al. 2012). For massive stars with identified pulsation modes, forward asteroseismic modelling is able to provide constraints on their (core) masses, ages, interior rotation profiles, and mixing properties (e.g. Aerts et al. 2003; Dupret et al. 2004; Salmon et al. 2022), but also probe the strength and geometry of an interior magnetic field (Lecoanet et al. 2022). A key goal of WG12 is to extract reliable TESS light curves, provide complementary constraints on the variability amplitudes and timescales of each XShootU target, and ultimately perform forward asteroseismic modelling (see Bowman 2020 for a review).

A.13. Magnetic Fields (WG13)

WG13 seeks to leverage the UV and optical spectral libraries provided by the ULLYSES and XShootU programmes to shed light on how magnetism affects massive star structure and evolution. In magnetic massive stars, which make up ~7% of the total OB star population (e.g. Morel et al. 2015; Wade et al. 2016; Grunhut et al. 2017), stable, nearly dipolar surface magnetic fields warp the stellar wind into a structurally complex magnetosphere, trapping the wind near the stellar surface, thus significantly altering the circumstellar environment. This magnetic wind confinement has been shown to reduce stellar mass-loss rate compared to non-magnetic stars of similar spectral type (ud-Doula et al. 2008). It should be noted that atypical features in P-Cygni profiles are not necessarily the result of a magnetic fields, as variability in the absorption components of wind-sensitive UV resonance lines have also been observed in non-magnetic massive stars (e.g. Massa et al. 1995; Kaper et al. 1996, 1999). The Erba et al. (2021) synthetic line profiles can be adapted for direct comparison with observations, and used in conjunction with the XShootU spectral libraries to identify new magnetic candidates.

A.14. Unusual Objects (WG14)

Finally, the data offer many opportunities to study key objects. For example, combining the radial velocities from XShootU with the exquisite proper motions from Gaia DR3, we can reconstruct the space motions of ULLYSES targets, which can be used to identify runaway and walkaway stars. Moreover, Gaia DR3 light-curves can be used in conjunction with radial velocities of known eclipsing binaries to estimate fundamental stellar parameters, providing unique tests of stellar evolution.

Appendix B: ULLYSES target parameters

In Table B.1 we present optical and NIR (JHK) photometry of the ULLYSES targets, as well as spectroscopic and multiplicity information. Table B.2 provides an extensive literature search for the stellar and wind parameters as they were known prior to the start of ULLYSES. Obviously, these data (see the excerpt of Table B.2; the full table is available at the CDS) are rather heterogeneous and they will quickly become outdated as new spectral analyses are underway.

Table B.1. Photometric, spectroscopic, and multiplicity of ULLYSES/XShootU targets, ordered by RA (Magellan/MIKE targets are indicated in the final column).

Target, Alias	Sp Type	Ref	U (mag)	B (mag)	V (mag)	Ref	J (mag)	H (mag)	K_s (mag)	Ref	$(B-V)_0$ (mag)	$E(B-V)$ (mag)	Ref	M_V (mag)	Binary?	Ref	MIKE?
SMC targets																	
2dFS 163	O8 Ib(f)	1	13.84	14.95	15.11	2	15.28	15.31	15.14	3,4	–0.27	0.11	5	–4.21	···	···	···
AzV 6, 2dFS 5002	O9 III	6	12.45	13.36	13.31	7	12.56	11.78	11.73	3,8	–0.26	0.31	5	–6.63	EB	9	···
AzV 14, Sk 9	O5 V	10	12.38	13.38	13.55	7	14.25	14.30	14.31	3,8	–0.28	0.11	5	–5.77	···	···	···
AzV 15, Sk 10	O6.5 II(f)	11	11.90	12.93	13.12	7	13.53	13.57	13.60	3,8	···	0.10	12	–6.17	···	···	···
AzV 16, Sk 11, R 4	sgB0[e]	13	12.29	13.10	12.97	7	12.35	11.73	11.35	3,8	···	0.07	14	–6.23	SB2	14	···
AzV 18, Sk 13	B2 Ia	6	11.70	12.49	12.46	15	12.47	12.36	12.32	3,8	–0.17	0.20	16	–7.16	···	···	✓
AzV 22, 2dFS 5015	B5 Ia	6	11.53	12.19	12.20	17	12.27	12.20	12.15	3,8	–0.09	0.08	16	–7.03	···	···	✓
AzV 39a, AB 2	WN5ha	18	13.08	14.08	14.26	7	14.67	14.64	14.64	3,4	···	0.10	19	–5.03	···	···	···
AzV 43, 2dFS 700	B0.5 III	20	12.80	13.76	13.88	7	14.37	14.33	14.48	3,8	···	0.08	12	–5.35	···	···	···
AzV 47	O8 III((f))	11	12.26	13.26	13.44	7	14.13	14.20	14.26	3,8	···	0.05	12	–5.70	···	···	···
AzV 61, Sk 32, 2dFS 748	O6 III((f))e	21	12.31	13.36	13.54	7	14.10	13.99	14.07	3,8	–0.27	0.09	5	–5.72	···	···	···
AzV 69, Sk 34	OC7.5 III((f))	11	12.09	13.09	13.27	7	13.76	13.77	13.86	3,8	···	0.11	12	–6.05	···	···	···
AzV 70, Sk 35, 2dFS 756	O9.5 Ibw	22	11.27	12.21	12.38	23	12.77	12.79	12.86	3,8	···	0.10	24	–6.91	···	···	···
AzV 75, Sk 38	O5 III(f^+)	11	11.55	12.55	12.70	7	13.15	13.22	13.22	3,8	···	0.14	12	–6.71	···	···	···
AzV 81, Sk 41, AB 4	WN6h	18	12.36	13.25	13.37	7	13.65	13.52	13.44	3,8	···	0.09	19	–5.89	···	···	···
AzV 80	O4-6n(f)p	11	12.22	13.19	13.32	7	13.80	13.74	13.87	3,8	–0.28	0.15	5	–6.13	···	···	···
AzV 83	O7 Iaf^+	11	···	13.45	13.58	11	13.87	13.96	13.90	3,8	–0.27	0.14	5	–5.83	···	···	✓
AzV 85	B1 II-IIIe	25	12.69	13.68	13.75	26	14.50	···	14.60	3	–0.24	0.17	16	–5.76	···	···	···
AzV 95	O7 III((f))	11	12.57	13.60	13.78	7	14.17	14.21	14.17	3,8	–0.27	0.09	5	–5.48	···	···	···
AzV 96, Sk 46, 2dFS 801	B1.5 Ia	6	11.54	12.49	12.59	7	12.93	12.98	12.95	3,8	–0.18	0.08	16	–6.64	···	···	✓
AzV 104	B0.5 Ia	6	12.05	13.01	13.17	7	13.65	13.71	13.73	3,8	–0.22	0.06	16	–6.00	···	···	✓
AzV 148	O8.5 V	27	12.92	13.92	14.12	7	14.67	14.78	14.80	3,4	···	0.09	28	–5.13	···	···	···
2dFS 999, AB 9	WN3 ha	18	14.13	15.12	15.24	7	15.84	15.92	15.78	3,4	···	0.09	19	–4.02	···	···	···
NGC330 ELS 4 = Rob B37	B2.5 Ib	29	···	13.26	13.33	29	13.44	13.45	13.46	3,8	–0.15	0.08	16	–5.90	···	···	✓
NGC330 ELS 2 = Rob A2	B3 Ib	29	12.07	12.80	12.87	7	13.07	13.09	13.08	3,8	–0.13	0.06	16	–6.30	···	···	✓
AzV 175, Sk 64	B1 IIw	30	12.61	13.45	13.53	7	13.83	13.87	13.89	3,8	–0.24	0.16	16	–5.95	···	···	✓

The infrared photometry is drawn from 2MASS (JHK_s) or VISTA VMC (JK_s). H-band photometry is missing if 2MASS and VISTA are discrepant (presumably due to photometric variability or sensitivity/crowding issues). References: **1** Evans et al. (2004b), **2** Zaritsky et al. (2002), **3** Cioni et al. (2011), **4** Cutri et al. (2012), **5** Martins & Plez (2006), **6** Lennon (1997), **7** Massey (2002), **8** Cutri et al. (2003), **9** Zasche et al. (2017), **10** Massey et al. (2004), **11** Walborn et al. (2000), **12** Bouret et al. (2021), **13** Lamers et al. (1998), **14** Zickgraf et al. (1996), **15** Ardeberg & Maurice (1977), **16** Fitzgerald (1970), **17** Ardeberg (1980), **18** Foellmi et al. (2003), **19** Hainich et al. (2015), **20** Lamb et al. (2013), **21** Lamb et al. (2016), **22** Walborn et al. (2002a), **23** Azzopardi et al. (1975), **24** Evans et al. (2004a), **25** Mennickent et al. (2006), **26** Azzopardi & Vigneau (1982), **27** Massey et al. (1995), **28** Bouret et al. (2013), **29** Evans et al. (2006), **30** Garmany et al. (1987), **31** Massey et al. (2005), **32** Walborn et al. (1995), **33** Massey et al. (1989), **34** Walborn et al. (2004), **35** Massey et al. (2009), **36** Dufton et al. (2019), **37** Heydari-Malayeri & Hutsemekers (1991), **38** Niemela (2002), **39** Shenar et al. (2016), **40** Koenigsberger et al. (2014), **41** Ritchie et al. (2012), **42** Walborn (1977), **43** Walborn (1983), **44** Pawlak et al. (2013), **45** Crampton & Greasley (1982), **46** Walborn et al. (2010), **47** Smith Neubig & Bruhweiler (1997), **48** Shenar et al. (2018), **49** Pauli et al. (2022), **50** Reynolds et al. (1993) **51** Ramachandran et al. (2019), **52** Sanduleak (1969), **53** Fitzpatrick (1991), **54** Schmidt-Kaler et al. (1999), **55** Urbaneja et al. (2017), **56** Ardeberg et al. (1972), **57** Fitzpatrick (1988), **58** Rousseau et al. (1978), **59** Smith et al. (1996), **60** Hainich et al. (2014), **61** Isserstedt (1979), **62** Parker et al. (1992), **63** Walborn et al. (2002b), **64** Massey et al. (2017), **65** Zaritsky et al. (2004), **66** Graczyk et al. (2011), **67** Morrell et al. (1999), **68** Smith et al. (1990), **69** Crowther et al. (2002a), **70** Crowther & Walborn (2011), **71** Schnurr et al. (2008), **72** Massey et al. (2000), **73** Crowther et al. (2002b), **74** Buscombe & Foster (1995), **75** Conti et al. (1986), **76** Blair et al. (2009), **77** Alcock et al. (1997), **78** Garmany & Walborn (1987), **79** Isserstedt (1982), **80** Isserstedt (1975), **81** Feitzinger & Isserstedt (1983), **82** Crowther & Smith (1997), **83** Crowther (2021, priv. com.), **84** Ostrov & Lapasset (2003), **85** Haefner et al. (1994), **86** Oey & Smedley (1998), **87** Garmany et al. (1994), **88** Ramachandran et al. (2018b), **89** Ramachandran et al. (2018a), **90** Evans et al. (2015b), **91** Negueruela & Coe (2002), **92** Hutchings et al. (1978), **93** Ulaczyk et al. (2013), **94** Mahy et al. (2020), **95** Evans et al. (2011), **96** Walborn et al. (2014), **97** Sana et al. (2013), **98** Shenar et al. (2022), **99** Parker (1993), **100** Selman et al. (1999), **101** Shenar et al. (2019), **102** Evans et al. (2015a), **103** Testor & Niemela (1998), **104** Fariña et al. (2009), **105** Gvaramadze et al. (2018), **106** Niemela & Gamen (2004), **107** Evans et al. (2007), **108** Lorenzo et al. (2022), **109** Massey et al. (2007),

Table B.1. continued.

Target, Alias	Sp Type	Ref	U (mag)	B (mag)	V (mag)	Ref	J (mag)	H (mag)	K_s (mag)	Ref	$(B-V)_0$ (mag)	$E(B-V)$ (mag)	Ref	M_V (mag)	Binary?	Ref	MIKE?
AzV 177	O4 V((f))	31	13.27	14.32	14.53	7	15.15	15.23	15.29	3,4	···	0.08	28	–4.70	···	···	···
AzV 186, NGC330 ELS 13	O8.5 III((f))	21	12.75	13.77	13.98	7	14.45	14.47	14.51	3,8	–0.27	0.06	5	–5.19	···	···	···
AzV 187, Sk 68	B3 Ia	6	11.21	11.96	12.06	15	12.29	12.23	12.29	3,8	–0.13	0.03	16	–6.13	···	···	✓
AzV 189, 2dFS 5096	O9 V	27	13.32	14.26	14.37	7	14.92	15.09	15.06	3,8	···	0.14	28	–5.03	···	···	···
AzV 200, Sk 69	B8 Ia	6	11.72	12.24	12.17	15	12.10	11.88	11.89	3,8	–0.01	0.08	16	–7.06	···	···	✓
NGC346 ELS 43 = MPG 11	B0 V	29	14.06	15.05	15.18	7	15.77	15.84	15.89	3,4	–0.30	0.17	16	–4.33	···	···	···
NGC346 ELS 26 = MPG 12	O9.5–B0 V (N str)	11	13.77	14.68	14.76	7	15.26	14.98	15.36	3,4	···	0.13	28	–4.64	···	···	···
NGC346 ELS 28 = MPG 113	OC6 Vz	11	13.56	14.62	14.78	7	15.46	15.52	15.62	3,4	···	0.09	28	–4.47	···	···	···
AzV 207	O7 III((f))	21	12.99	14.05	14.25	7	14.79	14.84	14.94	3,4	–0.27	0.07	5	–4.95	···	···	···
AzV 210, Sk 73	B1.5 Ia	6	11.73	12.58	12.6	7	12.80	12.77	12.79	3,8	–0.18	0.16	16	–6.88	···	···	✓
NGC346 ELS 50 = MPG 299	O8 Vn	29	13.93	15.09	15.25	7	16.05	16.37	16.22	3,4	···	0.05	28	–3.88	···	···	···
AzV 215, Sk 76, 2dFS 1352	BN0 Ia	6	11.64	12.60	12.69	7	13.01	12.99	13.04	3,8	–0.24	0.15	16	–6.76	···	···	···
NGC346 ELS 7 = MPG 324 = W6	O4 V((f))	32	12.73	13.78	14.02	33	14.53	14.66	14.68	3,4	···	0.07	28	–5.08	···	···	···
NGC346 MPG 355 = W3	ON2 III(f*)	34	12.15	13.27	13.50	33	13.98	14.11	14.14	3,4	···	0.07	28	–5.70	···	···	···
NGC346 MPG 368	O6 V	35	12.87	13.95	14.18	33	14.63	14.59	14.78	3,4	···	0.07	28	–5.01	···	···	···
NGC346 MPG 435 = W1	O4 If+O5-6	36	11.20	12.21	12.43	37	13.01	13.02	13.11	3,8	–0.28	0.06	5	–6.74	SB2	36,38	···
NGC346 ELS 51 = MPG 523	O7 Vz	29	14.20	15.25	15.51	29,33	16.01	16.07	16.16	3,8	···	0.05	28	–3.62	···	···	···
AzV 224, NGC346 ELS 8	B1 III	28	13.02	13.97	14.12	7	14.55	14.62	14.56	3,8	–0.26	0.11	16	–5.20	···	···	···
HD 5980, AzV 229, R 14, Sk 78, AB 5	WN6h+WNE+O	18	10.63	11.63	11.83	15	11.11	11.01	10.77	8	···	0.08	39	–7.30	SB2	40	···
NGC346 ELS 13 = MPG 782	O9 V+B1	41	13.36	14.28	14.46	33	14.95	···	15.05	3	–0.27	0.09	5	–4.80	SB2,EB	41,44	···
NGC346 ELS 46	O7 Vn	29	···	15.16	15.44	29	15.91	15.81	16.08	3,4	···	0.04	28	–3.66	···	···	···
AzV 232, Sk 80, NGC 346 ELS 1 = MPG 789	O7 Iaf$^+$	42	11.15	12.15	12.35	15	12.64	12.67	12.67	3,8	···	0.05	12	–6.79	···	···	···
AzV 234, Sk 81	B3 Iab	36	12.02	12.84	12.94	7	13.19	13.15	13.22	3,8	–0.13	0.03	16	–6.13	···	···	✓
AzV 235, R 17, Sk 82	B0 Iaw	43	11.07	12.02	12.20	23	12.41	12.32	12.28	3,8	···	0.07	24	–7.00	···	···	···
NGC346 ELS 35, 2dFS 1418	B1 V	29	13.83	14.70	14.89	7	15.48	15.73	15.63	3,4	–0.26	0.07	16	–4.31	EB	44	···
NGC346 ELS 25 = MPG 848	O9 V	29	13.67	14.67	14.91	33	15.47	15.59	15.63	3,4	–0.27	0.03	5	–4.16	···	···	···
NGC346 ELS 31	O8 Vz	29	13.65	14.74	14.96	7	15.59	15.67	15.75	3,4	···	0.09	28	–4.30	···	···	···
AzV 238	O9.5 III	11	12.49	13.47	13.64	7	14.25	14.26	14.35	3,8	–0.26	0.09	5	–5.62	···	···	···
AzV 243, Sk 84	O6 V	32	12.63	13.67	13.84	7	14.43	14.43	14.55	3,8	···	0.10	28	–5.44	···	···	···
AzV 242, R 18, Sk 85	B0.7 Iaw	43	11.03	11.95	12.06	15	12.42	12.33	12.38	3,8	–0.19	0.08	16	–7.17	···	···	···
AzV 251	O7.5 V	21	13.32	14.34	14.52	7	15.20	15.18	15.33	3,4	–0.27	0.09	5	–4.74	···	···	···
AzV 255, Sk 90	O8 V	27	11.58	12.59	12.78	15	13.47	13.41	13.13	3,8	–0.27	0.08	5	–6.45	···	···	···
AzV 261, 2dFS 1527	B2 Ibe	1	12.90	13.81	13.88	7	13.81	13.95	13.43	3,8	–0.16	0.09	16	–5.38	···	···	···
AzV 264, Sk 94	B1 Ia	6	11.33	12.24	12.37	15	12.75	12.76	12.75	3,8	–0.19	0.06	16	–6.80	···	···	✓
AzV 266, Sk 95, 2dFS 1545	B1 I	21	11.47	12.43	12.55	7	12.88	12.91	12.91	3,8	–0.19	0.07	16	–6.65	···	···	✓
AzV 267	O8 V	21	13.53	14.58	14.84	7	15.51	15.77	15.64	3,4	···	0.05	28	–4.29	···	···	···
AzV 296	O7.5 V((f))	10	13.05	14.07	14.26	7	14.90	14.91	15.00	3,4	–0.28	0.09	5	–5.00	···	···	···
AzV 304	B0.5 V	45	13.74	14.66	14.77	7	15.44	15.50	15.56	3,4	–0.28	0.17	16	–4.74	···	···	✓
AzV 307	O9 III	30	12.82	13.8	13.96	7	14.53	14.69	14.63	3,8	···	0.10	12	–5.33	···	···	···
AzV 314	B5 Iab	6	11.98	12.77	12.87	7	13.19	13.19	13.23	3,8	–0.10	0.00	16	–6.11	···	···	✓
AzV 321, 2dFS 1720	O9 IInp	46	12.54	13.57	13.76	7	14.32	14.38	14.41	3,8	–0.26	0.07	5	–5.44	···	···	···

Table B.1. continued.

Target, Alias	Sp Type	Ref	U (mag)	B (mag)	V (mag)	Ref	J (mag)	H (mag)	K_s (mag)	Ref	$(B-V)_0$ (mag)	$E(B-V)$ (mag)	Ref	M_V (mag)	Binary?	Ref	MIKE?
AzV 324	B4 Iab	47	12.11	12.79	12.84	7	13.09	13.07	13.10	3,8	–0.13	0.08	16	–6.39	···	···	✓
AzV 326	O9 V	27	12.84	13.80	13.92	7	15.08	···	15.25	3	···	0.06	28	–5.25	···	···	···
AzV 327, R 28	O9.5 II-Ibw	11	11.83	12.87	13.03	7	13.78	13.85	13.90	3,8	···	0.06	12	–6.14	···	···	✓
AzV 332, R 31, Sk 108, AB 6	WN3:h+O+O+O	48	11.11	12.14	12.37	15	12.95	13.02	13.03	3,8	···	0.08	48	–6.86	SB	48	···
AzV 343, Sk 111	B6 Iab	47	12.32	12.95	12.99	7	13.08	13.05	13.07	3,8	–0.07	0.03	16	–6.08	···	···	✓
AzV 362, R 36, Sk 114	B3 Ia	6	10.58	11.34	11.36	15	11.65	11.37	11.42	3,8	–0.13	0.11	16	–7.96	···	···	✓
AzV 372, Sk 116	O9.5 Iabw	22	11.41	12.44	12.59	7	13.04	13.07	13.08	3,8	···	0.12	24	–6.76	···	···	···
AzV 374	B2 Ib	6	12.04	12.91	13.04	7	13.46	13.48	13.53	3,8	–0.16	0.03	16	–6.03	···	···	✓
AzV 377, 2dFS 1971	O5 V((f))	1	13.19	14.25	14.45	7	15.21	15.18	15.33	3,4	–0.28	0.08	5	–4.78	···	···	···
AzV 388, 2dFS 2049	O4 V	30	12.81	13.88	14.09	7	14.67	14.76	14.80	3,4	·	0.08	28	–5.14	···	···	···
AzV 393, R 39, Sk 124	B1.5 Ia	30	10.55	11.41	11.43	15	11.88	···	11.60	3	–0.18	0.16	16	–8.05	···	···	✓
AzV 410	B0 III	30	12.11	13.06	13.21	7	13.75	13.77	13.83	3,8	–0.30	0.15	16	–6.24	···	···	···
2dFS 2266	OC7 II(f)	1	13.83	14.91	15.16	7	15.84	15.91	16.02	3,4	–0.27	0.02	5	–3.88	···	···	···
AzV 423, Sk 132, 2dFS 2319	O9.5 II(n)	22	12.08	13.08	13.25	7	13.76	13.82	13.83	3,8	–0.26	0.09	5	–6.01	···	···	···
AzV 435	O3 V((f*))	31	12.96	13.94	14.0	7	13.79	13.53	13.50	3,8	–0.28	0.22	5	–5.66	···	···	···
AzV 440	O8 V	31	13.30	14.30	14.48	7	15.12	15.17	15.27	3,4	–0.27	0.09	5	–4.78	···	···	···
AzV 445, Sk 138, 2dFS 2538	B5 Iab	6	11.90	12.65	12.71	7	12.92	12.93	12.94	3,8	–0.09	0.03	16	–6.36	···	···	✓
2dFS 2553	O6.5 III((f))e	21	13.82	14.82	14.95	7	15.27	15.04	15.07	3,4	–0.27	0.14	5	–4.46	···	···	···
AzV 446	O6.5 V	30	13.29	14.35	14.59	7	15.25	15.32	15.43	3,4	···	0.06	28	–4.59	···	···	···
AzV 456, Sk 143, 2dFS 2717	O9.5 Ibw	24	12.15	12.93	12.83	7	12.81	12.79	12.77	3,8	···	0.35	24	–7.24	···	···	···
AzV 468	O8.5 V	30	13.83	14.86	15.11	7	15.74	15.84	15.90	3,8	···	0.04	28	–3.99	···	···	···
AzV 469, Sk 148	O8.5 II((f))	22	11.91	12.96	13.12	7	13.58	13.63	13.68	3,4	···	0.09	24	–6.14	···	···	···
AzV 472, Sk 150, 2dFS 2907	B2 Ia	6	11.59	12.51	12.62	7	12.92	13.01	12.07	3,8	–0.17	0.06	16	–6.55	···	···	✓
AzV 476	O4 IV–II((f))p+O9.5:	49	12.50	13.43	13.52	7	13.72	13.72	13.76	3,8	···	0.26	49	–6.27	EB,SB2	44,49	···
AzV 479, Sk 155	O9 Ib	6	11.29	12.26	12.42	15	12.84	12.88	12.92	3,8	–0.26	0.10	5	–6.87	···	···	✓
AzV 488, Sk 159	B0.5 Iaw	43	10.79	11.76	11.89	15	12.26	12.18	12.24	3,8	···	0.09	24	–7.37	···	···	···
AzV 490, Sk 160, SMC X-1	B0 Iwp var	43	12.00	13.00	13.15	7	13.55	13.51	13.57	3,8	–0.24	0.09	16	–6.11	SB	50	···
AzV 506, Sk 169	B0.5 II	21	12.38	13.36	13.53	7	14.01	13.99	14.12	3,8	–0.28	0.11	16	–5.79	···	···	✓
[M2002] SMC 81469	O9.7 V	51	12.78	13.77	13.97	7	14.80	14.89	14.95	3,4	–0.26	0.06	5	–5.20	···	···	···
2dFS 3689, HV 2226	B1.5 V	51	14.12	15.11	15.25	7	15.73	15.86	16.00	3,4	–0.25	0.11	16	–4.07	EB	44	···
2dFS 3694	B1 IV	51	12.80	13.73	13.92	7	14.49	14.44	14.63	3,8	–0.26	0.07	16	–5.28	···	···	···
Sk 173, 2dFS 3747	B0.7 IIe	51	12.44	13.4	13.57	7	14.10	14.14	14.09	3,8	–0.24	0.07	16	–5.63	···	···	···
2dFS 3780	O9.7 IV	51	13.10	14.12	14.37	7	14.97	15.05	15.10	3,4	–0.26	0.01	5	–4.64	···	···	···
Sk 179	B6 I	52	12.24	12.96	13.06	7	13.32	13.33	13.37	3,8	–0.07	0.00	16	–5.92	···	···	✓
Sk 183	O3 V((f*))z	51	12.51	13.59	13.82	7	14.45	14.61	14.60	3,8	–0.28	0.05	5	–5.32	···	···	···
2dFS 3947	B1.5 IV	51	13.82	14.76	14.99	7	15.52	15.49	15.66	3,4	–0.28	0.02	16	–4.05	···	···	···
2dFS 3954	O6 V((f))z	51	13.93	15.01	15.27	7	15.88	16.08	16.05	3,4	–0.28	0.02	5	–3.77	···	···	···
Sk 187	O8.5 III	51	11.93	12.99	13.18	7	13.67	13.72	13.79	3,8	–0.27	0.08	5	–6.05	···	···	···
Sk 191	B1.5 Ia	6	10.97	11.82	11.86	15	12.03	11.96	11.90	3,8	–0.18	0.14	16	–7.55	···	···	···

Table B.1. continued.

Target, Alias	Sp Type	Ref	U (mag)	B (mag)	V (mag)	Ref	J (mag)	H (mag)	K_s (mag)	Ref	$(B-V)_0$ (mag)	$E(B-V)$ (mag)	Ref	M_V (mag)	Binary?	Ref	MIKE?
LMC targets																	
Sk –67° 2, HDE 270754, R 51	B1 Ia$^+$ (N wk)	53	10.49	11.30	11.26	54	12.24	11.00	11.01	3,8	···	0.20	55	–7.84	···	···	✓
Sk –67° 5, HDE 268605, R 53	O9.7 Ib	42	10.27	11.22	11.34	56	11.81	11.61	11.68	3,8	–0.26	0.14	5	–7.57	···	···	···
BI 13	O6.5 V	7	12.58	13.66	13.75	7	14.39	14.54	14.55	3,8	–0.27	0.18	5	–5.29	···	···	···
Sk –68° 8, HDE 268729, R 58	B5 Ia$^+$	57	10.39	11.09	11.02	54	12.31	10.87	11.16	3,8	–0.09	0.16	16	–7.96	···	···	✓
Sk –70° 13	O9 V	27	11.16	12.15	12.29	7	12.82	12.82	12.85	3,8	–0.27	0.13	5	–6.59	···	···	···
Sk –67° 14, HDE 268685	B1.5 Ia	22	10.51	11.42	11.52	56	12.08	11.78	11.90	3,8	···	0.08	55	–7.21	···	···	···
Sk –70° 16	B4 I	58	12.19	13.04	13.10	7	13.33	13.34	13.34	3,8	–0.13	0.07	16	–5.60	···	···	✓
Sk –67° 20, HD 32109, BAT99 7	WN4 b	59	12.89	13.53	13.79	7	13.26	13.10	12.75	3,8	···	0.08	60	–4.94	···	···	···
Sk –66° 17, N11 ELS 11	OC9.5 II	29	···	12.81	12.89	29	13.22	13.23	13.27	3,8	–0.26	0.18	5	–6.15	SB1	29	···
Sk –66° 18	O6 V((f))	27	12.23	13.30	13.50	61	13.99	13.97	14.09	3,8	–0.28	0.08	5	–5.23	···	···	···
Sk –69° 43, HDE 268809, R 65	B0.5 Ia	57	10.96	11.90	11.98	54	12.22	12.13	12.15	3,8	···	0.10	55	–6.81	···	···	···
N11 ELS 33, PGMW 1005, LH 9–89	B0 IIIn	29	12.57	13.46	13.68	62	14.02	14.05	14.08	3,8	–0.30	0.08	16	–5.05	···	···	···
N11 ELS 49, PGMW 1110, LH 9–73	O7.5 V	29	···	13.78	14.02	29	14.47	14.51	14.57	3,4	–0.27	0.03	5	–4.55	EB	44	···
N11 ELS 51	O5 Vn((f))	29	···	13.77	14.03	29	14.39	14.28	14.49	3,8	–0.28	0.02	5	–4.51	···	···	···
N11 ELS 18, PGMW 3053	O6 II(f$^+$)	29	···	13.04	13.13	29	13.33	13.31	13.35	3,8	–0.27	0.18	5	–5.91	···	···	···
N11 ELS 60, PGMW 3058	O3 V((f*))	63	13.18	14.18	14.24	62	14.70	14.22	14.29	3,8	–0.28	0.22	5	–4.92	···	···	···
N11 ELS 31, PGMW 3061, LH 10–3061	ON2 III(f*)	34	13.16	13.67	13.68	62	13.71	13.48	13.76	3,8	–0.28	0.27	5	–5.64	···	···	···
PGMW 3070	O6 V	62	11.84	12.53	12.75	62	12.42	12.42	12.42	4	–0.28	0.06	5	–5.92	···	···	✓
N11 ELS 46	O9.5 V	29	···	13.74	13.98	29	14.32	14.36	14.44	3,8	–0.26	0.02	5	–4.56	···	···	···
N11 ELS 38, PGMW 3100	O5 III(f$^+$)	29	12.89	13.81	13.81	62	13.75	13.77	13.70	3,8	–0.28	0.28	5	–5.54	···	···	···
PGMW 1363, BI 37, LH 9–34	O8.5 Iaf	62	11.66	12.61	12.69	54	12.88	12.86	12.86	3,8	–0.26	0.18	5	–6.35	···	···	···
PGMW 3120	O5.5 V((f*))	62	11.71	12.73	12.80	62	13.08	13.00	13.07	3,8	–0.28	0.21	5	–6.33	···	···	···
LMCe055-1	WN4 /O4	64	15.07	16.05	16.15	65	16.58	···	16.59	3	–0.28	0.18	5	–2.89	EB	66	···
N11 ELS 20	O5 Inf$^+$p	46	···	12.96	13.18	29	13.23	13.22	13.21	3,8	–0.28	0.06	5	–5.49	···	···	···
Sk –65° 2	B1 V	27	11.89	12.51	12.65	65	13.17	13.21	13.22	3,8	–0.26	0.12	16	–6.20	···	···	···
N11 ELS 26	O2.5 III(f*)	29	···	13.34	13.51	29	13.80	13.84	13.86	3,8	–0.28	0.11	5	–5.31	·	···	···
N11 ELS 32, PGMW 3168	O7 II(f)	29	12.58	13.57	13.68	62	13.81	13.79	13.18	3,8	–0.27	0.16	5	–5.30	···	···	···
N11 ELS 48, PGMW 3204	O6.5 V((f))	29	12.87	13.85	14.02	62	14.20	···	14.19	3	–0.27	0.10	5	–4.77	···	···	···
N11 ELS 13, PGMW 3223, BI 42	O8 V	29	11.87	12.83	12.93	62	13.17	13.19	13.18	3,8	–0.27	0.17	5	–6.08	···	···	···
Sk –66° 35, HDE 268732	BC1 Ia	53	10.62	11.52	11.61	54	11.70	11.74	11.69	3,8	···	0.09	54	–7.15	SB1	67	✓
Sk –69° 50	O7(n)(f)p	46	12.16	13.15	13.31	7	13.60	13.67	13.66	3,8	–0.27	0.11	5	–5.51	···	···	···
Sk –68° 15, HD 32402, BAT99 11	WC4	68	12.19	12.77	12.90	7	13.32	13.22	12.69	8	···	0.11	69	–5.92	···	···	···
Sk –67° 22, BAT99 12	O2 If*/WN5	70	12.21	13.26	13.44	7	13.81	13.78	13.81	3,8	–0.28	0.10	5	–5.35	SB1	71	···
Sk –68° 16, LH 12–43	O7 III	72	11.68	12.66	12.85	7	13.36	13.43	13.45	3,8	–0.27	0.08	5	–5.88	···	···	···
Sk –69° 52, HDE 268867	B2 Ia	57	10.73	11.55	11.50	56	11.73	11.57	11.58	3,8	–0.17	0.22	16	–7.66	···	···	···
Sk –70° 32	O9.5 II:	57	11.84	12.85	13.06	7	13.49	13.56	13.59	3,8	–0.26	0.05	5	–5.58	···	···	···
Sk –68° 23a	B1 III	27	12.03	12.97	13.05	7	13.25	13.24	13.24	3,8	–0.26	0.18	16	–5.99	···	···	···

Table B.1. continued.

Target, Alias	Sp Type	Ref	U (mag)	B (mag)	V (mag)	Ref	J (mag)	H (mag)	K_s (mag)	Ref	$(B-V)_0$ (mag)	$E(B-V)$ (mag)	Ref	M_V (mag)	Binary?	Ref	MIKE?
Sk –65° 22, HDE 270952	O6 Iaf$^+$	42	10.85	11.88	12.07	61	12.35	12.36	12.34	3,8	···	0.07	73	–6.63	···	···	···
Sk –68° 26	BC2 Ia	53	10.98	11.75	11.64	54	11.60	11.26	11.27	3,8	···	0.22	55	–7.52	···	···	✓
Sk –66° 50, HDE 268907, R 73	B8 Ia$^+$	53	9.98	10.65	10.63	56	10.48	10.44	10.40	8	···	0.07	55	–8.07	···	···	✓
Sk –70° 50, HDE 269009	B3 Ia	53	10.45	11.16	11.20	56	11.22	11.27	11.22	8	–0.13	0.09	16	–7.56	···	···	✓
Sk –70° 60	O4–5 V((f))pec	35	12.63	13.72	13.88	7	14.16	14.27	14.00	3,8	–0.28	0.12	5	–4.97	···	···	···
Sk –70° 69	O5.5 V((f))	35	12.63	13.72	13.95	7	14.40	14.51	14.52	3,8	–0.28	0.05	5	–4.69	···	···	···
Sk –68° 41	B0.5 Ia	57	10.97	11.90	12.04	74	12.23	12.30	12.24	8	···	0.06	55	–6.63	···	···	···
Sk –70° 79	B0 III	27	11.70	12.65	12.71	7	12.74	12.74	12.70	3,8	–0.30	0.24	16	–6.51	···	···	···
Sk –68° 52, HDE 269050, R 78	B0 Ia	42	10.69	11.66	11.72	54	11.84	11.75	11.72	3,8	···	0.17	24	–7.29	···	···	···
Sk –71° 8, LH 28-12	O9 II	75	12.15	13.11	13.25	61	13.51	13.52	13.57	3,8	–0.26	0.12	5	–5.60	···	···	✓
HV 5622	B0 V	76	14.09	14.61	14.85	65	15.20	15.18	15.40	3,4	–0.30	0.06	16	–3.82	EB	77	···
Sk –67° 51	O6.5 III	75	11.53	12.48	12.68	65	13.03	13.07	13.16	3,8	–0.27	0.07	5	–6.02	···	···	···
Sk –67° 69	O4 III(f)	78	11.88	12.93	13.09	61	13.52	13.64	13.60	3,8	–0.28	0.12	5	–5.76	···	···	···
Sk –69° 83, HDE 269244	O7.5 Iaf	57	10.45	11.47	11.61	54	11.86	11.89	11.92	8	–0.27	0.13	5	–7.27	···	···	···
BI 128	O9 V	27	12.55	13.57	13.82	79	14.33	14.34	14.41	3,8	–0.27	0.02	5	–4.72	···	···	···
Sk –69° 104, HDE 269357	O6 Ib(f)	42	10.86	11.89	12.10	56	12.53	12.62	12.63	3,8	–0.27	0.06	5	–6.57	···	···	···
Sk –67° 78, HDE 269371	B3 Ia	53	10.49	11.22	11.26	56	11.60	11.45	11.35	3,8	···	0.06	55	–7.41	···	···	✓
Sk –65° 47, LH 43–18	O4 I(n)f$^+$p	46	11.27	12.33	12.51	80	12.95	12.90	12.98	3,8	–0.28	0.10	5	–6.28	···	···	···
Sk –65° 55, BAT99 30	WN6 h	59	12.16	13.14	13.36	81	13.27	13.12	12.92	3,8	···	0.07	60	–5.34	···	···	···
Sk –71° 19, LH 50–5	O6 III	75	13.15	14.03	14.23	65	14.77	14.87	14.85	3,8	–0.27	0.07	5	–4.47	···	···	···
Sk –71° 21, HD 36063, BAT99 32	WN6(h)	82	11.48	12.46	12.71	81	12.61	12.46	12.36	3,8	···	0.08	60	–6.02	SB	71	···
Sk –68° 73, HDE 269445, R 99, BAT99 33	WN9pec	83	10.92	11.72	11.45	80	10.54	10.32	10.01	8	···	0.37	60	–8.18	···	···	···
Sk –67° 101, LH 54–21	O8 II((f))	22	11.41	12.44	12.67	7	13.05	13.05	13.13	3,8	–0.27	0.04	5	–5.93	···	···	···
Sk –67° 105	O4 f+O6	84	11.25	12.28	12.42	85	12.71	12.60	12.77	3,8	–0.28	0.14	5	–6.49	SB2	84	···
Sk –67° 106, HDE 269525	O8 III((f))	86	10.76	11.8	11.96	86	12.33	12.35	12.39	3,8	–0.27	0.11	5	–6.86	···	···	✓
Sk –67° 107	O9 Ib(f)	86	11.49	12.51	12.67	86	13.02	13.08	13.06	3,8	–0.26	0.10	5	–6.12	···	···	✓
Sk –67° 108	O4-5 III	57	11.33	12.37	12.57	7	13.07	13.06	13.15	3,8	–0.28	0.08	5	–6.16	·	···	···
LH 58–496	O5 V((f))	72	12.41	13.51	13.73	87	14.20	14.28	14.31	3,8	–0.28	0.06	5	–4.94	···	···	···
Sk –67° 111, LH 60–53	O6 Ia(n)fpv	46	11.33	12.39	12.60	7	12.95	12.95	13.02	3,8	–0.27	0.06	5	–6.07	…	···	···
BI 173	O8 II:	22	11.78	12.8	12.96	7	13.24	13.27	13.30	3,8	–0.27	0.11	5	–5.86	···	···	···
Sk –67° 118	O7 V	27	11.76	12.79	12.98	7	13.52	13.59	13.65	3,8	–0.27	0.08	5	–5.75	···	···	✓
Sk –69° 140	B4 I	58	11.66	12.61	12.71	7	13.00	12.98	13.07	3,8	–0.13	0.03	16	–5.86	···	···	✓
Sk –66° 100	O6 II(f)	32	11.99	13.05	13.26	61	13.74	13.75	13.84	3,8	–0.27	0.06	5	–5.41	···	···	···
Sk -71° 35	B1 II	88	11.94	12.88	12.97	7	13.09	13.22	13.05	3,8	···	0.12	88	–5.88	···	···	···
BI 184	O8 (V)e	88	12.80	13.76	13.84	7	13.68	13.90	13.63	3,8	···	0.17	88	–5.17	···	···	···
Sk –71° 41	O9.7 Iab	88	11.78	12.75	12.82	7	12.94	12.98	12.91	3,8	···	0.16	88	–6.16	···	···	···
NGC2004 ELS 3, R 109	B5 Ia	29	11.26	11.97	12.05	54	12.21	12.12	12.09	3,8	–0.09	0.01	16	–6.46	···	···	✓
BI 189	O8 IV((f))e	89	12.45	13.39	13.45	7	13.40	13.40	13.26	3,8	–0.27	0.21	5	–5.68	···	···	···
N206–FS 170	B1 IV	88	13.63	14.22	14.39	65	14.91	14.86	15.01	3,4	–0.26	0.09	16	–4.37	···	···	···

Table B.1. continued.

Target, Alias	Sp Type	Ref	U (mag)	B (mag)	V (mag)	Ref	J (mag)	H (mag)	K_s (mag)	Ref	$(B-V)_0$ (mag)	$E(B-V)$ (mag)	Ref	M_V (mag)	Binary?	Ref	MIKE?
Sk –71° 45, HDE 269676, R 113	O4–5 III(f)	42	10.41	11.43	11.57	54	12.39	···	12.40	3	–0.28	0.14	5	–7.34	···	···	···
Sk –67° 166, HDE 269698, R 115	O4 If$^+$	42	11.04	12.05	12.27	56	12.70	12.67	12.72	3,8	···	0.08	73	–6.46	···	···	···
Sk –71° 46	O4 If	27	12.37	13.26	13.27	27	13.02	12.93	12.99	3,8	–0.28	0.27	5	–6.05	EB	66	···
Sk –67° 167, LH 76–21	O4 Inf$^+$	78	11.24	12.31	12.53	7	12.90	12.88	12.94	3,8	–0.28	0.06	5	–6.14	···	···	···
Sk –67° 168, HDE 269702	O8 I(f)p	46	10.91	11.91	12.08	80	12.48	12.51	12.58	3,8	–0.27	0.10	5	–6.71	···	···	···
Sk –69° 178	O9.2 II	90	12.13	13.17	13.26	65	13.62	13.64	13.77	3,8	–0.26	0.17	5	–5.75	·	···	···
LMC X-4	O8 III	91	···	13.94	14.17	65	14.63	14.65	14.67	3,4	–0.27	0.04	5	–4.43	SB1	92	···
Sk –67° 191	O8 V	75	12.21	13.25	13.46	61	13.77	13.82	13.84	3,8	–0.27	0.06	5	–5.21	···	···	···
Sk –67° 195	B6 I	58	12.21	12.82	12.84	7	12.81	12.73	12.68	3,8	–0.07	0.05	16	–5.80	···	···	✓
Sk –67° 197	B7 I	58	11.63	12.35	12.34	7	12.05	11.93	11.84	3,8	–0.04	0.05	16	–6.30	···	···	✓
Sk –66° 152, HDE 271366	O7 Ib(f)	57	11.33	12.38	12.58	54	12.93	12.92	12.96	3,8	–0.27	0.07	5	–6.12	···	···	···
Sk –69° 191, HD 37680, BAT99 61	WC4	68	12.98	12.92	13.01	72	13.30	12.67	13.26	3,8	···	0.13	69	–5.87	···	···	···
W61 28–5	O4 V((f$^+$))	10	12.64	13.74	13.92	72	14.29	14.36	14.44	3,8	–0.28	0.10	5	–4.87	···	···	···
W61 28–23	O3.5 V((f$^+$))	31	12.52	13.65	13.81	72	14.16	14.20	14.24	3,8	–0.28	0.12	5	–5.04	···	···	···
Sk –67° 207, HDE 269801, R 121	B9 Ia	57	10.04	10.57	10.51	56	10.31	10.20	10.20	8	0.00	0.06	16	–8.16	···	···	✓
Sk –67° 211, HDE 269810, R 122	O2 III(f*)	63	11.03	12.10	12.28	54	12.79	12.79	12.87	3,8	–0.28	0.10	5	–6.51	···	···	···
MCPS 083.91120-69.69685	O3 If*	90	12.34	13.14	13.28	65	13.69	13.77	13.78	3,8	–0.28	0.14	5	–5.63	···	···	···
Sk –67° 216	B0.5 V	27	11.70	12.68	12.84	61	13.19	13.16	13.23	3,8	–0.28	0.12	16	–6.01	···	···	···
Sk –69° 212	O5n(f)p	46	11.31	12.26	12.31	72	12.48	12.39	12.47	3,8	–0.28	0.23	5	–6.88	EB	93	···
BI 237	O2 V((f*))	31	12.80	13.77	13.89	7	14.00	14.01	13.99	3,8	–0.28	0.16	5	–5.09	···	···	···
Sk –68° 133	OC3.5 III(f*)	90	12.02	13.03	13.15	7	13.32	13.32	13.39	3,8	–0.28	0.16	5	–5.83	···	···	···
Sk –66° 171, HDE 269889	O9 Ia	57	11.02	12.04	12.19	80	12.62	12.57	12.62	3,8	–0.26	0.11	5	–6.63	···	···	···
LMCe078–1	O6 Ifc	64	12.49	13.46	13.49	65	13.68	···	13.75	3	–0.27	0.24	5	–5.73	···	···	✓
VFTS 66	O9 V+B0.2 V	94	···	15.64	15.54	96	15.21	···	15.10	3	–0.27	0.37	5	–4.09	SB2	94	···
VFTS 72, BI 253	O2 V-III(n)((f*))	95	12.65	13.67	13.76	7	13.80	13.77	13.81	3	–0.28	0.19	5	–5.31	···	···	···
Sk –68° 135, HDE 269896, R 129	ON9.7 Ia$^+$	42	10.50	11.36	11.36	56	11.46	11.24	11.16	3,8	···	0.25	24	–7.90	···	···	···
VFTS 169, [ST92] 1–71	O2.5 V(n)((f*))	96	···	14.62	14.59	95	14.07	13.98	13.90	3,8	–0.28	0.31	5	–4.85	···	···	···
VFTS 180, [ST92] 1–78, LH 99–3, BAT99 93	O3 If*	70	···	13.46	13.54	95	13.40	13.29	13.34	3,8	–0.28	0.20	5	–5.56	···	···	···
VFTS 190	O7 Vnn((f))p	96	···	14.63	14.67	95	14.66	14.68	14.66	3,4	–0.27	0.23	5	–4.52	···	···	···
VFTS 244	O5 III(n)(fc)	96	···	13.94	14.04	95	14.04	14.03	14.03	3,8	–0.28	0.18	5	–5.00	···	···	···
VFTS 267	O3 III-I(n)f*	96	···	13.44	13.49	95	13.34	13.27	13.30	3,8	–0.28	0.23	5	–5.70	···	···	···
Sk –68° 137	O2 III(f*)	34	12.24	13.22	13.29	7	13.35	13.33	13.41	3,8	–0.28	0.21	5	–5.84	···	···	···
VFTS 355	O4 V((n))((fc))z	96	···	13.93	14.12	95	14.33	14.43	14.42	3,8	–0.28	0.09	5	–4.64	SB2	97	···
VFTS 404	O3.5: V:((fc))+O5 V:	98	···	14.16	14.14	95	13.75	13.73	13.66	3,8	–0.28	0.30	5	–5.27	SB2	98	···
VFTS 406, Mk 55	O6 Vnn	96	13.67	14.31	14.30	99	14.15	14.21	14.07	3,8	–0.28	0.29	5	–5.08	···	···	···
VFTS 482, Mk 39, BAT99 99	O2.5 If*/WN6	70	12.12	12.97	12.85	100	12.37	···	12.09	3	–0.28	0.40	5	–6.87	SB2	83	···
VFTS 506, Mk 25	ON2 V((n))((f*))	96	12.47	13.32	13.31	100	13.04	12.84	12.97	3,8	–0.28	0.29	5	–6.07	···	···	···

Table B.1. continued.

Target, Alias	Sp Type	Ref	U (mag)	B (mag)	V (mag)	Ref	J (mag)	H (mag)	K_s (mag)	Ref	$(B-V)_0$ (mag)	$E(B-V)$ (mag)	Ref	M_V (mag)	Binary?	Ref	MIKE?
BAT99 105, Mk 42	O2 If*	70	11.84	12.71	12.71	99	12.33	···	12.10	3	–0.28	0.28	5	–6.64	···	···	···
VFTS 542, Mk 30, BAT99 113	O2 If*/WN5 + B0	101	12.67	13.56	13.47	100	13.03	···	12.86	3	–0.28	0.37	5	–6.16	SB2	101	···
VFTS 545, Mk 35, BAT99 114	O2 If*/WN5	70	12.66	13.52	13.4	100	12.90	···	12.70	3	–0.28	0.40	5	–6.32	···	···	···
VFTS 586	O4 V((n))((fc))z	96	···	14.92	15.04	95	14.95	14.84	14.85	3,4	–0.28	0.16	5	–3.94	···	···	···
Sk –68° 140, VFTS 696	B0.7 Ib-Iab Nwk	102	11.99	12.84	12.79	7	12.51	12.43	12.41	3,8	–0.16	0.24	16	–6.43	···	···	···
HDE 269927c, Sk –69° 249c, BAT99 120	WN9h	82	11.53	12.50	12.63	103	12.50	12.37	12.24	3,8	···	0.15	60	–6.32	···	···	···
[ST92] 5–52, W61 3–14	O3V ((f*))+OB	63	12.37	13.26	13.41	103	13.84	13.86	13.94	3,8	–0.28	0.13	5	–5.47	···	···	···
[ST92] 5–27, W61 3–24	O3 V((f))	72	13.48	14.48	14.58	103	14.92	14.89	14.99	3,4	–0.28	0.18	5	–4.46	···	···	···
[ST92] 4–18, W61 4–4	O5 If	72	12.63	13.64	13.66	72	13.77	13.77	13.78	3,8	–0.28	0.26	5	–5.63	···	···	···
BI 265, Farina 82	O5 III(fc)	90	11.42	12.43	12.58	54	12.70	12.72	12.79	3,8	–0.28	0.13	5	–6.30	···	···	···
Farina 88, MCPS 085.03420-69.65476	O4 III(f)	104	12.87	13.56	13.63	65	13.86	13.82	13.92	3,8	–0.28	0.21	5	–5.50	···	···	✓
Sk –71° 50	O6.5 III	75	12.31	13.32	13.44	61	13.73	13.76	13.82	3,8	–0.27	0.15	5	–5.51	···	···	···
Sk –69° 279	O9.2 Iaf	105	12.00	12.84	12.79	80	12.62	12.58	12.50	3,8	–0.26	0.31	5	–6.65	···	···	···
Sk –68° 155	B0.5 I	58	11.84	12.74	12.75	7	12.63	12.64	12.60	3,8	–0.24	0.23	16	–6.44	···	···	···
LH 114–7	O2 III(f*)+OB?	63	12.27	13.41	13.66	7	14.12	14.26	14.38	4	–0.28	0.03	5	–4.91	···	···	···
BI 272	O7 II	75	12.05	13.06	13.28	79	13.72	13.79	13.86	3,8	–0.27	0.05	5	–5.36	···	···	✓
Sk –67° 261	O8.5 III	27	11.47	12.29	12.40	65	12.82	12.79	12.84	3,8	–0.27	0.16	5	–6.58	···	···	···
Sk –67° 266, S 61, BAT99 133	WN11h	82	10.93	11.88	12.01	56	12.11	12.00	11.82	3,8	···	0.11	60	–6.81	···	···	···
Sk –70° 115, HDE 270145, LH 117-43	O6 If+O8:	106	11.16	12.14	12.24	80	12.37	12.30	12.33	3,8	–0.27	0.17	5	–6.77	SB2	106	···
NGC 3109 targets																	
NGC 3109 EBU 07, SC88 B138	B0–1 Ia	107	···	···	18.69	107	···	···	···	···	···	0.09	107	–7.16	···	···	···
NGC 3109 EBU 20	O8 I	107	···	···	19.33	107	···	···	···	···	–0.27	···	5	···	···	···	···
NGC 3109 EBU 34	O8 I(f)	107	···	···	19.61	107	···	···	···	···	–0.27	···	5	···	···	···	···
Sextans A targets																	
Sextans A GHN s4 LGN22 s004	O5 III	108	19.44	20.64	20.92	109	···	···	···	···	–0.28	0.00	5	–4.71	···	···	···
Sextans A GHN s2, LGN22 s003	O3–5 Vz	108	19.52	20.71	20.80	109	···	···	···	···	–0.28	0.19	5	–5.42	···	···	···
Sextans A LGN22 s071	B0 I	108	18.39	19.46	19.70	109	···	···	···	···	–0.24	0.00	16	–5.93	···	···	···

Table B.2. Pre-ULLYSES target parameters compiled by the ULLYSES team at STScI. Excerpt only. The full table is available at the CDS.

Target	SpType	Ref	$T_{\rm eff}$ (K)	Ref	log g (cgs)	Ref	log $L/L_\odot$	Ref	$R/R_\odot$	Ref	$M/M_\odot$	Ref	$v \sin i$ (km s^{-1})	Ref	$v_{\rm inf}$ (km s^{-1})	Ref	$\dot{M}$ ($M_\odot$ yr^{-1})	Ref
SMC targets																		
2dFS 163	O8 Ib(f)	1	-	-	-	-	-	-	-	-	-	-	-	-	-	-	-	-
AzV 6	O9 III	2	-	-	-	-	-	-	-	-	-	-	-	-	-	-	-	-
AzV 14	O5 V	3	44000	3	4.0	3	5.82	3	14.2	3	74.0	3	261	4	2000	3	1.0E-07	3
AzV 15	O6.5 II(f)	5	39000	6	3.6	6	5.83	6	18.0	From L,Teff	47.2	6	120	6	2050	6	1.1E-06	6
AzV 16	sgB0[e]	7	-	-	-	-	-	-	-	-	-	-	-	-	-	-	-	-
AzV 18	B2 Ia	2	19000	8	2.3	8	5.44	8	49.0	8	28.0	8	49	8	325	9	2.3E-07	8
AzV 22	B5 Ia	2	14500	8	1.9	8	5.04	8	53.0	8	19.0	8	46	8	280	8	2.3E-07	8
AzV 39a	WN5ha	10	47000	11	-	-	5.57	11	9.1	11	43.0	11	-	-	900	11	1.8E-06	11
AzV 43	B0.5 III	12	28500	6	3.4	6	5.13	6	15.1	From L,Teff	22.4	6	200	6	1200	6	2.2E-08	6
AzV 47	O8 III((f))	5	35000	6	3.8	6	5.44	6	14.3	6	42.2	6	60	6	2000	6	2.1E-08	6
AzV 61	O6 III((f))e	13	-	-	-	-	-	-	-	-	-	-	228	4	2025	14	-	-
AzV 69	OC7.5 III((f))	5	33900	6	3.5	6	5.61	6	18.6	From L,Teff	39.7	6	70	6	1800	6	9.8E-07	6
AzV 70	O9.5 Ibw	15	28500	16	3.1	16	5.68	16	28.4	16	-	-	100	16	1450	16	1.5E-06	16
AzV 75	O5 III(f+)	5	38500	6	3.5	6	5.94	6	21.0	From L,Teff	51.1	6	120	6	2050	6	1.6E-06	6
AzV 81	WN6h	10	45000	11	-	-	5.78	11	13.0	11	38.0	11	-	-	1000	11	6.6E-06	11
AzV 80	O4-6n(f)p	5	38000	17	3.5	17	-	-	-	-	-	-	325	17	1550	9	-	-
AzV 83	O7 Iaf+	5	32800	6	3.3	6	5.54	6	18.3	From L,Teff	22.1	6	80	6	940	6	2.3E-06	6
AzV 85	B1 II-IIIe	18	-	-	-	-	-	-	-	-	-	-	-	-	-	-	-	-
AzV 95	O7 III((f))	5	38200	19	3.7	19	5.56	19	13.8	19	39.3	19	68	19	1700	9	3.6E-07	19
AzV 96	B1.5 Ia	2	22000	20	2.6	20	5.39	20	34.0	20	27.0	20	90	20	850	20	2.4E-07	20
AzV 104	B0.5 Ia	2	27500	8	3.1	8	5.31	8	20.0	8	26.0	8	80	8	1340	8	4.0E-07	8
AzV 148	O8.5 V	21	32300	22	4.0	22	4.84	22	8.4	From L,Teff	19.0	22	60	22	1540	22	2.0E-09	22
2dFS 999	WN3 ha	10	100000	11	-	-	6.05	11	3.5	11	-	-	-	-	1800	11	2.2E-06	11
NGC330 ELS 4	B2.5 Ib	23	17000	24	2.3	24	4.77	24	28.0	From L,Teff	15.0	24	41	24	-	-	-	-
NGC330 ELS 2	B3 Ib	23	14590	24	2.2	24	4.73	24	36.3	From L,Teff	15.0	24	14	24	-	-	-	-
AzV 175	B1 IIW	25	-	-	-	-	-	-	-	-	-	-	51	4	-	-	-	-
AzV 177	O4 V((f))	26	44500	22	4.0	22	5.43	22	8.7	From L,Teff	38.8	22	220	22	2400	22	1.4E-07	22
AzV 186	O8.5 III((f))	13	34500	19	3.4	19	5.40	19	14.1	19	32.2	19	73	19	1600	19	3.0E-07	19
AzV 187	B3 Ia	2	-	-	-	-	-	-	-	-	-	-	-	-	-	-	-	-
AzV 189	O9 V	21	32300	22	4.0	22	4.81	22	8.1	From L,Teff	18.8	22	150	22	1250	22	6.0E-10	22
...	...	..	...	..	..	..	...	..	...	...	...	..	...	..	...	..	...	..

References. **1** Evans et al. (2004b), **2** Lennon (1997), **3** Massey et al. (2004), **4** Penny & Gies (2009), **5** Walborn et al. (2000), **6** Bouret et al. (2021), **7** Lamers et al. (1998), **8** Trundle et al. (2004), **9** Evans et al. (2004c), **10** Foellmi et al. (2003), **11** Hainich et al. (2015), **12** Lamb et al. (2013), **13** Lamb et al. (2016), **14** Prinja & Crowther (1998), **15** Walborn et al. (2002a), **16** Evans et al. (2004a), **17** Heap et al. (2006), **18** Mennickent et al. (2006), **19** Mokiem et al. (2006), **20** Trundle & Lennon (2005), **21** Massey et al. (1995), **22** Bouret et al. (2013), **23** Evans et al. (2006), **24** Trundle et al. (2007), **25** Garmany et al. (1987), **26** Massey et al. (2005), **27** Hosek (2014), **28** Hunter et al. (2007), **29** Walborn et al. (1995), **30** Walborn et al. (2004), **31** Massey et al. (2009), **32** Dufton et al. (2019), **33** Hunter et al. (2008b), **34** Shenar et al. (2016), **35** Ritchie et al. (2012), **36** Walborn (1977), **37** Walborn (1983), **38** Puls et al. (1996), **39** Castro et al. (2018), **40** Crampton & Greasley (1982), **41** Hunter et al. (2005), **42** Rolleston et al. (2003), **43** Walborn et al. (2010), **44** Smith Neubig & Bruhweiler (1997), **45** Shenar et al. (2018), **46** Dufton et al. (2005), **47** Dufton et al. (2006), **48** Rivero González et al. (2012a), **49** Ramachandran et al. (2019), **50** Bell et al. (1991), **51** Sanduleak (1969), **52** Fitzpatrick (1991), **53** Urbaneja et al. (2017), **54** Penny et al. (2004), **55** Massey (2002), **56** Fitzpatrick (1988), **57** Rousseau et al. (1978), **58** Smith et al. (1996), **59** Hainich et al. (2014), **60** Mokiem et al. (2007a), **61** Rivero González et al. (2012b), **62** Walborn et al. (2002b), **63** Parker et al. (1992), **64** Massey et al. (2017), **65** Massey et al. (2000), **66** Crowther et al. (2002a), **67** Crowther & Walborn (2011), **68** Crowther et al. (2002b), **69** Conti et al. (1986), **70** Blair et al. (2009), **71** Garmany & Walborn (1987), **72** Massa et al. (2003), **73** Schnurr et al. (2008), **74** Crowther & Smith (1997), **75** Crowther (2021, priv. com.), **76** Ostrov & Lapasset (2003), **77** Oey & Smedley (1998), **78** Ramachandran et al. (2018b), **79** Ramachandran et al. (2018a), **80** Evans et al. (2015b), **81** Negueruela & Coe (2002), **82** Mahy et al. (2020), **83** Walborn et al. (2014), **84** Bestenlehner et al. (2014), **85** Ramírez-Agudelo et al. (2013), **86** Ramírez-Agudelo et al. (2017), **87** Sabín-Sanjulián et al. (2017), **88** Ramírez-Agudelo et al. (2013), **89** Shenar et al. (2019), **90** Sabín-Sanjulián et al. (2014), **91** Evans et al. (2015a), **92** McEvoy et al. (2015), **93** Fariña et al. (2009), **94** Gvaramadze et al. (2018), **95** Niemela & Gamen (2004), **96** Evans et al. (2007), **97** Tramper et al. (2014), **98** Garcia et al. (2019), **99** Garcia (2019, priv. com.).